Received: 25 December 2023 | Revised: 25 November 2024 | Accepted: 16 December 2024

DOI: 10.1111/bph.17448

RESEARCH ARTICLE

Novel FKBP prolyl isomerase 1A (FKBP12) ligand promotes functional improvement in SOD1^{G93A} amyotrophic lateral sclerosis (ALS) mice

Laura Moreno-Martinez[1,2,3,4] | Núria Gaja-Capdevila[1,5] | Laura Mosqueira-Martín[1,6,7] | Mireia Herrando-Grabulosa[1,5] | Laura Rodriguez-Gomez[7] | Klaudia Gonzalez-Imaz[1,6,7] | Ana C. Calvo[1,2,3,4] | Maialen Sagartzazu-Aizpurua[8] | Leticia Moreno-García[1,2,3,4] | Jose Manuel Fuentes[1,9,10] | Abraham Acevedo-Arozena[1,11] | Jesús María Aizpurua[8,12] | José Ignacio Miranda[8,12] | Adolfo López de Munain[1,6,7,12,13] | Ainara Vallejo-Illarramendi[1,6,7,12] | Xavier Navarro[1,5] | Rosario Osta[1,2,3,4] | Francisco Javier Gil-Bea[1,7,12,14,15]

[1]Centro de Investigación Biomédica en Red Sobre Enfermedades Neurodegenerativas (CIBERNED), Madrid, Spain

[2]LAGENBIO, Faculty of Veterinary, University of Zaragoza, Zaragoza, Spain

[3]Aragón Health Research Institute (IIS Aragón), Biomedical Research Centre of Aragón (CIBA), Zaragoza, Spain

[4]AgriFood Institute of Aragon-IA2 (UNIZAR-CITA), Zaragoza, Spain

[5]Department of Cell Biology, Physiology and Immunology, Institute of Neurosciences, Universitat Autònoma de Barcelona, Bellaterra, Spain

[6]Group of Neurosciences, Departments of Pediatrics and Neuroscience, Faculty of Medicine and Nursing, University of Basque Country (UPV/EHU), San Sebastian, Spain

[7]Department of Neuroscience, BioGipuzkoa Health Research Institute (IIS BioGipuzkoa), San Sebastian, Spain

[8]Department of Organic Chemistry-I, Korta Research Center, University of the Basque Country (UPV/EHU), San Sebastian, Spain

[9]Department of Biochemistry and Molecular Biology and Genetics, Faculty of Nursing and Occupational Therapy, University of Extremadura, Cáceres, Spain

[10]Instituto de Investigación Biosanitaria de Extremadura (INUBE), Cáceres, Spain

[11]Research Unit, Canarias University Hospital, ITB-ULL, Tenerife, Spain

[12]Miramoon Pharma, San Sebastian, Spain

[13]Donostia University Hospital, San Sebastian, Spain

[14]IKERBASQUE Basque Foundation for Science, Bilbao, Spain

[15]Department of Health Sciences, Public University of Navarra, Pamplona, Spain

Abbreviations: ALS, amyotrophic lateral sclerosis; ER, endoplasmic reticulum; MP-001, 4-[[(3-Methoxyphenyl)thio]methyl]-1H-1,2,3-triazole-1-acetic acid; MP-004, 4-[[(4-Methoxyphenyl)thio]methyl]-N,N-dimethyl-1H-1,2,3-triazole-1-ethanamine); MP-010, 4-[[(4-Methoxyphenyl)sulfinyl]methyl]-N,N-dimethyl-1H-1,2,3-triazole-1-ethanamine; NMJ, neuromuscular junction; SOD1, superoxide dismutase 1.

Laura Moreno-Martinez, Núria Gaja-Capdevila and Laura Mosqueira-Martín have equal contribution.

Correspondence
Xavier Navarro, Rosario Osta and Francisco Javier Gil-Bea, Centro de Investigación Biomédica en Red Sobre Enfermedades Neurodegenerativas (CIBERNED), 28031 Madrid, Spain.
Email: xavier.navarro@uab.cat; osta@unizar.es and fransciscojavier.gilbeas@bio-gipuzkoa.eus

Funding information
This work was funded by project CIBER-CALS PI2020/08-1, Grants CB06/05/1105 and CB06/05/0041 from the Instituto de Salud Carlos III of Spain, Grants PID2022-140354OB-I00 and PID2020-119780RB-100 from the Agencia Estatal de Investigación, co-funded by European Union (NextGenerationEU, Recovery, Transformation and Resilience Plan), and Grant IT1732-22 from the Basque Government - Eusko Jaurlaritza. F. J. G.-B. was funded by Fundacion Roche Stop Fuga de Cerebros programme (BIO19/ROCHE/017/BD) and received support from the IKERBASQUE, Basque Foundation for Science (IKERBASQUE/PP/2022/003). L. M.-M. holds a PhD fellowship from the Euskal Herriko Univertsitatea (UPV/EHU) (PIF19/184). Open access funding provided by Universidad Pública de Navarra.

Background and Purpose: Amyotrophic lateral sclerosis (ALS) is a devastating neurodegenerative disease with limited treatment options. ALS pathogenesis involves intricate processes within motor neurons, characterized by dysregulated Ca^{2+} influx and buffering in early ALS-affected motor neurones. This study proposes the modulation of ryanodine receptors (RyRs), key mediators of intracellular Ca^{2+}, as a therapeutic target.

Experimental Approach: A novel class of novel FKBP12 ligands that show activity as cytosolic calcium modulators through stabilizing RyR channel activity, were tested in the superoxide dismutase 1 $(SOD1)^{G93A}$ mouse model of ALS. Different outcomes were used to assess treatment efficacy, including electrophysiology, histopathology, neuromuscular function and survival.

Key Results: Among the novel FKBP12 ligands, MP-010 was chosen for its central nervous system availability and favourable *in vitro* pharmaco-toxicological profile. Chronic administration of MP-010 to $SOD1^{G93A}$ mice produced preservation of motor nerve conduction, with the 61-$mg{\cdot}kg^{-1}$ dose significantly delaying the onset of motor impairment. This was accompanied by improved motor coordination, increased innervated endplates and significant preservation of motor neurones in the spinal cord of treated mice. Notably, MP-010 treatment significantly extended lifespan by an average of 10 days compared to vehicle.

Conclusions and Implications: FKBP12 ligands, particularly MP-010, exhibit promising neuroprotective effects in ALS, highlighting their potential as novel therapeutic agents. Further investigations into the molecular mechanisms and clinical translatability of these compounds are needed for their application in ALS treatment.

KEYWORDS
ALS, calcium, FKBP12, RyR, SOD1

1 | INTRODUCTION

Amyotrophic lateral sclerosis (ALS) is a devastating neurodegenerative disease that targets both upper and lower motor neurons within the brain and spinal cord. Tragically, ALS is characterized by a brief survival span of 2–3 years, with only 10%–20% of patients surpassing a decade of life post-diagnosis. Familial cases, attributable to genetic mutations, account for 5%–10% of all ALS cases, with the rest classified as sporadic (Mead et al., 2023). Despite intense ongoing research, current medications such as **riluzole**, **edaravone**, **tauroursodeoxycholic acid (TUDA; Relyvrio®)** and **tofersen (Qalsody®)** provide only a modest delay in disease progression. The pathogenesis of ALS is a complex interplay of multiple processes occurring within motor neurones, encompassing among other proposed mechanism: excitotoxicity, endoplasmic reticulum (ER) stress, mitochondrial dysfunction, oxidative stress, RNA processing aberrations, protein misfolding, endosomal trafficking disruptions, impaired axonal transport or neuroinflammation (Es et al., 2017; Zhou & Xu, 2023). Computational models have underscored the significance of disturbances in calcium (Ca^{2+}) homeostasis and energy imbalances as pivotal factors predicting neuronal dysfunction and degeneration in ALS (LeMasson et al., 2014).

One distinguishing feature in early ALS-affected motor neurones is the excessive influx of Ca^{2+} ions due to high-frequency rhythmic activity and an increased expression of Ca^{2+}-permeable **AMPA receptors** (Bursch et al., 2019; Guatteo et al., 2007). These motor neurones exhibit low expression of Ca^{2+} buffering proteins like parvalbumin and calbindin (Alexianu et al., 1994; Ince et al., 1993). Overexpression of these proteins has been shown to confer resistance to ALS-induced toxicity in motor neurones (Ho et al., 1996). Conversely, motor neurones that exhibit resistance to ALS degeneration, such as those of oculomotor and Onuf's nuclei, possess higher levels of Ca^{2+} buffering proteins (Elliott & Snider, 1995; Vanselow & Keller, 2000). Notably, ALS-associated mutations, including those in *VAPB VAMP* (vesicle-associated membrane protein-associated protein B and *C gene*), **SIGMAR1 (sigma non-opioid intracellular receptor 1 gene)** and *SOD1* (superoxide dismutase 1 gene) can potentiate Ca^{2+} deregulation and heighten vulnerability to the effects of Ca^{2+} influx (De Vos et al., 2012; Bernard-Marissal et al., 2015; Leal & Gomes, 2015; Petrozziello et al., 2022). These findings emphasize the inherent susceptibility of motor neurones to intracellular Ca^{2+} overload as a significant risk factor for degeneration (Appel et al., 2001).

Mitochondria play a pivotal role in regulating intracellular Ca^{2+} levels through the mitochondrial uniporter, particularly crucial in motor neurones with low intrinsic cytosolic Ca^{2+} buffering capacity. In these vulnerable motor neurones, mitochondria are responsible for absorbing over 50% of intracellular Ca^{2+} increases, setting them apart from other cell types. Consequently, the pronounced demand placed on specialized Ca^{2+} storage organelles make motor neurones even more susceptible to Ca^{2+} imbalances (Bergmann & Keller, 2004; Jaiswal, 2013), especially in ALS where mitochondria are frequently damaged (Zhou & Xu, 2023). Indeed, impaired mitochondrial Ca^{2+} buffering in motor neurones derived from patient-induced pluripotent stem cells carrying mutations in *TARDBP* (transactive response DNA binding protein 43 gene) or *C9orf72* (chromosome 9 open reading frame 72 gene) has been reported (Dafinca et al., 2020).

Apart from excessive Ca^{2+} influx and diminished Ca^{2+} buffering capacity, augmented Ca^{2+} leakage from ER stores in motor neurones can further contribute to cytosolic Ca^{2+} overload. **Ryanodine receptors (RyRs)** are tetrameric channels that play a crucial role in mediating Ca^{2+}-induced Ca^{2+} release from the ER, play a crucial role in this process (Fabiato, 1983; McPhersonx et al., 1991). RyR channels are activated by Ca^{2+} and can also be triggered by the oxidation of redox-sensing thiols by reactive oxygen species (ROS), creating a positive feedback loop exacerbating pathological cytoplasmic Ca^{2+} overload (Zima & Mazurek, 2016). The endogenous ligand of the RyR, FKBP prolyl isomerase 1A (FKBP12; calstabin), normally stabilizes RyR, preventing Ca^{2+} leakage from the ER. Reduced FKBP12 levels in motor neurones of ALS patients underscore the importance of maintaining equilibrium between FKBP12 and RyR in neurodegeneration (Kihira et al., 2005).

Overall, this cumulative evidence suggests the prospect of RyRs as a potential therapeutic target for ameliorating intracellular Ca^{2+} dysregulation and forestalling Ca^{2+}-induced neurodegeneration within susceptible neurons and neuromuscular units in ALS. In this context, we introduce a novel class of triazole molecules, empirically validated as FKBP12 ligands to facilitate FKBP12-RyR binding. This binding capability serves to stabilize the Ca^{2+} flux mediated by RyR, as demonstrated in our previous works (Aizpurua et al., 2021; Passannante et al., 2023). In this study, we introduce MP compounds, novel FKBP12 ligands that exhibit cytosolic calcium modulating activity, with the potential to be used for the treatment of ALS. This proposal is based on the encouraging results observed in transgenic $SOD1^{G93A}$ mice, a mouse model that recapitulates the key clinical, electrophysiological and histopathological features of the disease. (Mancuso et al., 2011; Turner & Talbot, 2008).

What is already known?

- Increased intracellular calcium levels contribute to the pathogenesis of amyotrophic lateral sclerosis (ALS).
- Targeted therapy towards modulating intracellular calcium homeostasis may have potential in treating ALS.

What does this study add?

- A novel class of FKBP12 ligands showing neuroprotection in the $SOD1^{G93A}$ mouse model of ALS.
- Demonstrates the potential therapeutic impact of stabilizing RyR channel activity for ALS treatment.

What is the clinical significance?

- Stabilizing RyR channel activity presents a promising avenue for ALS treatment with implications for disease progression.

2 | METHODS

2.1 | Detection of primary MP-010 metabolites in liver microsomes

To investigate the primary metabolic pathways of MP-010, liver microsomes from both mouse and human were incubated with the test compound (10 μM) at 37°C for 60 min. The metabolic activity of the liver microsomes was validated using the positive control 7-ethoxycoumarin (10 μM). Following incubation, samples were analysed by high-performance liquid chromatography coupled with ultraviolet and high-resolution mass spectrometry (HPLC-UV/MS). The structures of the detected metabolites were proposed based on their MS and tandem mass spectrometry (MS^2) data, and compared to reference standards. In addition to unchanged MP-010, four primary metabolites (M1-M4) were identified. Accurate mass measurements were obtained for all compounds and the relative abundance of MP-010 and its metabolites was calculated based on peak area analysis under the UV spectrum (234–274 nm) or MS peak area, relative to the total area of all drug-related components.

2.2 | Recordings of endoplasmic reticulum (ER) and cytoplasmic Ca^{2+} in HEK293 cells

HEK293 cells (RRID:CVCL_0045), stably and inducible-expressing WT and mutant R2474S-RyR2, were generated as described (Murayama et al., 2015) and provided by Dr. Takashi Murayama (Juntendo University). Cells co-express R-CEPIA1er (calcium-measuring organelle-Entrapped Protein IndicAtor 1 in the ER), a calcium-measuring organelle-entrapped protein indicator located at the ER, and they have an inducible expression for wild-type RyR2 and mutant RyR2 R2473S isoforms. 60.000 cells per well were

seeded onto 96-well plates coated with 50-μg·ml^{-1} poly-D-Lysine, as described previously (Murayama et al., 2015). Cells were grown in 10% FBS, DMEM media, at 37°C and 5% CO2 for 24 h. On Day 2, RyR expression was induced with 2-μg·ml^{-1} doxycycline. Induction was achieved after 24–28 h, when calcium measurements were performed in HEPES-buffered Krebs solution (140-mM NaCl, 5-mM KCl, 1-mM $MgCl_2$, 2-mM CaCl2, 11 mM D-[+]-glucose, 5-mM HEPES, distilled H2O to 450 ml, pH 7.4). Fluorescent ratios (F/F0) were calculated as the ratio of the fluorescence intensities between the initial (F0) and the last (F) 100 s by R-CEPIA1er in the Glomax Discover Microplate Reader (Promega). **Caffeine**-induced Ca^{2+} waves were also measured with Fura-2 AM at room temperature using an ECLIPSE Ti/L100 epifluorescence microscope (Nikon) equipped with a 20X S-Fluor objective, a lambda-DG4 illumination system, an Orca-Flash 2.8 camera (Hamamatsu) and NisElements-AR software. Fluorescence intensity ratios (F340/F380) were calculated to quantify changes in cytosolic Ca^{2+} levels.

2.3 | Rat cortical primary neurons

Cortical primary neurons were isolated from embryonic day 16 (E16) rat embryos. The pregnant rats were euthanised by exposure to $CO_2$and neck dislocation. After the embryos were euthanised *ex utero* by rapid decapitation, their brains were quickly removed and placed in sterile cold phosphate-buffered saline (PBS). The cortices were dissected and minced into small pieces. The tissue pieces were then subjected to gentle mechanical trituration to obtain a single-cell suspension. Cells were resuspended in neurobasal medium supplemented with B27, glutamax and antibiotics. Viable cells were counted using a haemocytometer and plated onto polyethylenimine (PEI) and Geltrex-coated Ibidi well plates at a density of approximately 1×10^4 cells per well for Ca^{2+} imaging, or onto CytoView MEA 24-well plates (Axion Biosystems) at a density of approximately 1×10^5 cells per well for microelectrode array recordings. Cultures were maintained at 37°C in a humidified atmosphere with 5% CO_2, with half the medium replaced every 2–3 days.

2.4 | Recordings of cytoplasmic Ca^{2+} load in rat cortical neurons

To determine the effect of the compound MP-004 on cytosolic Ca^{2+}levels following an insult that induces calcium leakage through RyRs, we employed the oxidative agent hydrogen peroxide (H_2O_2) at a concentration of 100 μM. Neurons were incubated with Fura-2 AM in a physiological imaging buffer for 30 min at 37°C. Following the loading period, excess Fura-2 AM was washed out and the cells were allowed to equilibrate for an additional 10 min. Baseline Ca^{2+} levels were measured for 3 min prior to the application of H_2O_2. After baseline measurements, cells were treated with 100 μM H_2O_2. Subsequent to treatment, calcium levels were re-evaluated by recording fluorescence for an additional 3 min, starting 30 s post-treatment. The analysis included four groups of cells: Control and MP-010 at 0.5, 5 or 50 μM. Within three experiments, data were obtained from 17 (Control), 21 (0.5 μM), 25 (5 μM) and 30 neurons (50 μm). Ca^{2+} imaging was performed as specified for HEK293 cells.

2.5 | Recordings of cytoplasmic Ca^2 transients in rat cortical neurons

Primary cortical neurons were loaded with the Ca^{2+}-sensitive fluorescent dye Fluo-8 AM and pluronic acid for 30 min 37°C. Following the incubation, the cells were washed to remove any excess dye. Fluo-8 fluorescence signals were acquired using the same microscope employed for Fura-2 AM acquisitions, but at a sampling rate of 5 Hz. This experiment included four groups of cells: Control and MP-010 at 0.5, 5 or 50 μM. Within three experiments, data were obtained from 35 (Control), 29 (0.5 μM), 55 (5 μM) and 37 neurons (50 μm). A custom R script was used to identify peaks in the fluorescence time series. Peaks were defined as local maxima that exceeded a predefined threshold. For each identified peak, a time interval of 3 s was extracted to capture the decay phase of the Ca^{2+} transient. The *x*-values (time) within each interval were normalized to start at zero and the y-values (fluorescence) were scaled to a range of 0 to 1, for consistent comparison of decay kinetics. An exponential decay model was then fitted to the normalized fluorescence data using nonlinear regression. The model parameters included the initial fluorescence value (*y*0, corresponding to the transient peak) and the decay time constant (tau). The fitted tau value, representing the time constant of the Ca^{2+} transient decay, was extracted for each peak. The normalized data was plotted using *ggplot2*, with individual neuron traces displayed in grey and a smoothed trendline representing the overall signal of each group in the corresponding colour.

2.6 | *In vitro* neurotoxicity assessment

Neurotoxicity assessment compound MP-010 was conducted using microelectrode array (MEA) assays, which offer enhanced sensitivity compared to conventional metabolic or viability endpoints. Many neurotoxins induce acute effects on neuronal network behaviour that are not adequately captured by traditional methods (Defranchi et al., 2011). In this study, we evaluated the effects of increasing concentrations of the compound on rat primary cortical neurons cultured in microelectrode array plates. Key parameters were measured, including mean firing rate, which indicates neuronal functionality, network burst frequency, which reflects the integrity of synapses, and synchronicity index, which indicates overall network activity. The assessment involved both chronic treatments over 10 days and acute treatments lasting 1 h. The experimental design included various treatment groups:- control and MP-010 at concentrations of 0.5, 5 and 50 μM, as well as different MP-010 metabolites (M1-M4) at the concentration of 10 μM. Each

treatment group was replicated four-six times, with each replicate consisting of a well containing neurons derived from an independent embryo.

2.7 | *In vitro* cardiotoxicity assessment

iCell Cardiomyocytes^2 (Fujifilm Cellular Dynamics, #C1058) were thawed and plated in gelatin-coated Z-plates at a density appropriate for subsequent experiments. The plating medium was utilized according to the manufacturer's recommendations. Approximately 4 to 24 h post-seeding, the media was replaced with maintenance medium to promote optimal growth conditions for the cardiomyocytes. At 48 h post-seeding, MP-010 dose–response curves were prepared in triplicate. Subsequently, cardiomyocytes were treated with MP-010 and impedance measurements were recorded post-treatment to assess cytotoxicity. Impedance measurements were performed using the Maestro Z system (Axion Biosystems), enabling real-time monitoring of cellular responses to the compound. The data were analysed to determine cytotoxic effects based on changes in impedance values relative to baseline measurements. Bright-field images and video recordings were obtained 19 h after treatment to evaluate changes in cell morphology and behaviour in response to MP-010 exposure. The experimental design included various treatment groups:- MP-010 at concentrations of 20 mM, 10 mM, 6 mM, 3 mM, 500 μM and 50 μM. Each treatment group was replicated 3 times.

2.8 | *In vivo* pharmacokinetics in mice

A bolus of 30 mg·kg^{-1} of test compounds were administered via oral gavage to control mice under general anaesthesia induced and maintained with 1.5-2.5% isoflurane. Body temperature was maintained using homeothermic blanket. Tissue samples, including muscle, brain and serum were collected at 2-, 4-, 6- and 18-h post-administration, from three mice at each time point, after mice were euthanised humanely by blood withdrawal under deep anaesthesia. Collected tissues were promptly preserved at −80°C until further processing. Frozen muscle and brain samples were pulverized in liquid nitrogen using a steel mortar immersed in dry ice. Approximately 100 mg of pulverized tissue and 100 μl of serum were then incubated with a 1% formic acid-acetonitrile solution, with equal volumes of tissue mass for muscle and brain, and three times for serum. Following a 90-s ultrasound bath for muscle and a 10-s bath for serum and brain samples, the extracts underwent centrifugation at 9600*g* and 4°C for 5 min. The resulting supernatants were collected and stored at −80°C until further quantification. Quantitative determination of compounds in the biological samples was carried out using liquid chromatography–tandem mass spectrometry (LC-MS/MS) at the Research General Services SGIker of UPV/EHU (Vitoria-Gasteiz). The pharmacokinetic parameters following oral administration were calculated using the PKSolver add-in programme (Zhang et al., 2010). Noncompartmental analysis was employed to compute the pharmacokinetic parameters of the parent compound. The terminal slope was automatically estimated using regression with the largest adjusted R^2. The parameters inferred included the terminal half-life ($t_{1/2}$), maximum concentration (C_{max}) and the time taken to reach the maximum concentration (T_{max}). Subsequently, the brain-to-serum (Cb:Cs) was calculated based on the obtained pharmacokinetic parameters (Shaffer, 2010).

2.9 | Animals and experimental design: treatment of SOD1^{G93A} mice

We used the hybrid strain of SOD1^{G93A} mouse as an ALS model (B6SJL-Tg[SOD1-G93A]1Gur; Strain #:002726, RRID:IMSR_JAX:002726). Non-transgenic wild-type (WT) littermates were used as controls. The animals used were from colonies that had been bred in different animal facilities for years, as specified below. The transgenic offspring was identified by polymerase chain reaction (PCR) amplification of DNA extracted from the tail, to identify hemizygous transgenic mice and WT. The colony was maintained under standard conditions (food and water *ad libitum*, room temperature of 22 ± 2°C and 12:12-h light–dark cycle) in conventional cages (ref. 1145T, Tecniplast, Italy) with a maximum of 5 mice per cage, at the Animal Service of the UAB and at the animal facilities in Centro de Investigación Biomédica de Aragón University of Zaragoza. Animal studies are reported in compliance with the ARRIVE guidelines (Percie du Sert et al., 2020) and with the recommendations made by the *British Journal of Pharmacology* (Lilley et al., 2020). All experimental procedures were approved by the Ethics Committee of the Universitat Autònoma de Barcelona (CEEAH-UAB: 2969 and 4273) and by the Ethics Committee for Animal Experiments from the University of Zaragoza (PI45/18, PI15/21, PI51/21 and PI02/23). Humane endpoint criterium in the survival studies was considered when animals lost the righting reflex for longer than 30 s.

2.9.1 | Trial 1: Effect of MP-010 on neuromuscular outcomes

This trial was conducted at the animal facility of the Universitat Autònoma de Barcelona using the colony of SOD1^{G93A} mice that has been bred over years by Dr. Navarro's group. At 8 weeks of age (before drug treatment started), WT and SOD1^{G93A} mice were randomly allocated to six experimental groups, according to their progenitors, sex, weight and electrophysiology baseline values in balanced groups for the assessment of neuromuscular outcomes:- (1) WT vehicle, this group consists of WT mice with no treatment (n = 8; 4 females + 4 males); (2) WT MP-010 61 mg·kg^{-1} (n = 9; 5 + 4); (3) WT MP-010122 mg·kg^{-1} (n = 5; 2 + 3); (4) SOD1^{G93A} vehicle (n = 16; 8 + 8); (5) SOD1^{G93A} MP-010 61 mg·kg^{-1} (n = 15; 7 + 8); (6) SOD1^{G93A} MP-010122 mg·kg^{-1} (n = 9; 5 + 4). The compound MP-010 was added to the drinking water at concentrations of 1 or 2 mM, resulting in average daily dosages of 61 or 122 mg·kg^{-1}, respectively. Daily water consumption was monitored weekly to determine the necessary compound concentration, which was

estimated at 5 ml·day^{-1} per animal, consistent with previous reports (Bachmanov et al., 2002). The treatment was given from the eighth until the 16th week of age and electrophysiological, behavioural and histological analyses were performed during this follow-up.

2.9.2 | Trial 2: Effect of MP-010 on survival, behavioural tests and genetic markers

This trial was conducted at the animal facility of the University of Zaragoza using the colony of SOD1^{G93A} mice that has been bred for years by Dr. Osta's group. The mice were randomly allocated to two groups: (1) SOD1^{G93A} MP-010 61 mg·kg^{-1} (n = 21; 8 + 13); (2) SOD1^{G93A} vehicle (n = 20; 9 + 11 females/males). The treatment started at 8 weeks of age and was weekly renewed until each mouse reached its respective humane endpoint. Throughout the treatment, all mice underwent weekly weight measurements and motor behavioural tests, including rotarod and hanging-wire tests. All behavioural experiments were conducted under blind conditions regarding the treatment.

2.9.3 | Trial 3: Effect of MP-001 on survival, behavioural tests and genetic markers

This trial was conducted at the animal facility of the University of Zaragoza using the colony of SOD1^{G93A} mice that has been bred for years by Dr. Osta's group. The mice were randomly allocated to two groups:- (1) SOD1^{G93A} MP-001 61 mg·kg^{-1} (n = 19; 9+10); (2) SOD1^{G93A} vehicle (n = 17; 9+8). All mice underwent weekly weight measurements and behavioural tests, including rotarod and hanging-wire tests, and the survival time was monitored. All behavioural experiments were conducted under blind conditions regarding the treatment.

2.10 | Functional evaluation of treated SOD1^{G93A} mice

2.10.1 | Rotarod

The Rotarod test (ROTA-ROD/RS, LE8200, LETICA, Scientific Instruments; Panlab, Barcelona, Spain) was conducted on a weekly basis, spanning from 8/9 to 16 weeks of age or until mice were unable to perform the test in the case of mice from the survival experiment, to assess the motor coordination, muscle strength and balance of the experimental animals. Specifically, the test involved measuring the duration for which each mouse could maintain its position on a rotating rod set at a constant speed of 14 rpm. Each animal underwent a series of five trials and the longest latency achieved without falling was recorded. An arbitrary cut-off time of 180 s was applied in the assessment. The symptomatic disease onset for each mouse was determined as the first week when the mouse was unable to keep walking 180 s on the rod.

2.10.2 | Hanging-wire test

Hanging-wire test was carried out in mice involved in the survival study to assess the muscular strength. Briefly, each mouse was placed on an inverted wire lid and the time it took for the mouse to fall was recorded. Similar to the rotarod test, the mice had three attempts to remain on the wire for a maximum of 180 s per trial and the longest latency was noted.

2.11 | Nerve conduction tests in treated SOD1^{G93A} mice

Motor nerve conduction tests were performed by percutaneously sciatic nerve stimulation (with single square pulses of 20-μs duration) delivered through a pair of needle electrodes placed at the sciatic notch. Compound muscle action potentials were recorded from the tibialis anterior and plantar interossei muscles utilizing microneedle electrodes. Recorded potentials were amplified and displayed with settings adjusted to measure amplitude from baseline to the maximal negative peak, latency from the stimulus to the onset of the first negative deflection and the duration of the wave (Gaja-Capdevila et al., 2021; Mancuso et al., 2011). Throughout the tests, pentobarbital (50 mg·kg^{-1} i.p.) was used to anaesthetise and the mice body temperature was maintained at a constant level using a thermostatic heating pad. The mice were spontaneously breathing during the tests. Electrophysiological tests were conducted at 8 (prior to the initiation of drug administration), 12, 14 and 16 weeks of age.

2.12 | Histology of treated SOD1^{G93A} mice

At the 16-week of age mice killed with an overdose of pentobarbital and underwent transcardial perfusion with a 4% paraformaldehyde solution. Following perfusion, the lumbar segment of the spinal cord was carefully extracted, post-fixed for 2 h and subsequently cryopreserved in a solution of 30% sucrose in phosphate buffer (PB) at 4°C. Then, transverse 20-μm-thick sections of the spinal cord were serially cut with a cryostat. For assessing the number of motor neurones, slices of L4-L5 spinal cord segments separated 100 μm were stained with a solution of 3.1-mM cresyl violet for 3 h. Motor neurones were identified by their anatomical localization in the ventral horn of the spinal cord and counted following strict criteria of their size (diameters lager than 20 μm) and morphological characteristics (polygonal shape and prominent nucleoli).

To assess glial cells immunoreactivity in the lumbar spinal cord, endogenous peroxidase activity was inhibited (70% methanol, 30% TBS, 2% H_2O_2) followed by blocking solution (1.5% normal horse serum and 1% BSA in TBS-Triton). Slides were incubated overnight at 4°C with primary antibodies anti-Iba1 (1:500; FUJIFILM Wako Pure Chemical Corporation Cat# 019-19741, RRID:AB_839504) and anti-GFAP (1:500; Thermo Fisher Scientific Cat# 13-0300, RRID:AB_2532994) to label microglia and astroglia, respectively. After washing,

slides were incubated with secondary antibodies anti-Rat IgG (H + L) biotinylated made in goat (1:200; Vector Laboratories Cat# BA-9400, RRID:AB_2336202) and anti-Rabbit IgG (H + L) biotinylated made in horse (1:200; Vector Laboratories Cat# BA-1100, RRID:AB_2336201) for 1 h. Afterwards, the slides were incubated with VECTASTAIN® Elite ABC-HRP Kit (Vector; pk6100) and finally, with DAB solution (SK-4100, Vector) for brown staining. Slides were dehydrated and mounted with DPX. To quantify glial cell reactivity, the percentage of area occupied by glial fibrillary acidic protein (GFAP) or allograft inflammatory factor 1 (Iba1/AIF1) immunolabelling was measured using ImageJ software. All the immuno-related procedures used comply with the recommendations made by the *British Journal of Pharmacology* (Alexander et al., 2018).

2.13 | Neuromuscular junction assessment in treated SOD1^{G93A} mice

After perfusion, the tibialis anterior muscle was collected and underwent cryoprotection in PB 30% sucrose solution. To label neuromuscular junctions (NMJ), the muscle was sectioned in longitudinal slices of 50 µm thickness, collected in sequential series. Following a blocking step using 5% normal donkey serum, the sections were incubated for 48 h at 4°C with primary antibodies, chicken anti-neurofilament 200 (NF200, 1:1000; Millipore Cat# AB5539, RRID:AB_11212161) and rabbit anti-synaptophysin (1:500; Abcam Cat# ab32127, RRID:AB_2286949). After washing steps, the sections were incubated overnight with secondary antibodies Alexa Fluor 594-conjugated secondary antibody (1:200); (Thermo Fisher Scientific Cat# A-11042, RRID:AB_2534099; Cat# A-21207, RRID:AB_141637) and Alexa Fluor 488-conjugated α-bungarotoxin (1:500; Thermo Fisher Scientific Cat# B35451, RRID:AB_2617152). The prepared slides were then mounted using ProLong. Fluoromount G Mounting Medium (RRID:SCR_015961). Images were captured under confocal microscopy (LSM 700 Axio Observer, Carl Zeiss, 20X with a numerical aperture of 0.5) and maximum projection images were generated from z projections with a thickness of 1.3 µm. To evaluate the proportion of innervated NMJs, each individual endplate was classified as either occupied (when presynaptic terminals covered the endplate) or vacant (when there was no presynaptic label in contact with the endplate). A total of at least 60 endplates from four different fields were analysed for each mouse.

2.14 | Protein extraction and FKBP12.6 and RyR protein expression in spinal cords of SOD1G93A mice

Protein was extracted from mouse spinal cord using RIPA lysis buffer (50 mM Tris–HCl pH 7.2, 0.9% NaCl, 1% NP40, 1-mM EGTA, 1-mM EDTA) containing protease and phosphatase inhibitors (#748443, Thermo Fisher) and inhibitors of calpain I/II and cathepsins B/L (#208719, Sigma). Protein quantification was performed by Bradford protein assay (#500-0006, Bio-Rad). Capillary Western blot was performed using the Jess instrument (ProteinSimple, Biotechne), following the manufacturer's instructions. Protein samples were diluted to 0.5–2 $\mu g \cdot \mu l^{-1}$ with 5X Fluorescence Master Mix (Biotechne) and denatured at 95°C for 5 min. Samples were loaded onto customary plates (#SM-W004 or #SM-W005, Biotechne) for protein separation. Primary antibodies used were: FKBP12.6 Antibody (R&D Systems Cat# AF4174, RRID:AB_2246838) and Anti-Ryanodine Receptor 2/RyR2 Antibody (Alomone Labs Cat# ARR-002, RRID:AB_2040184). Secondary antibodies used were: Anti-Goat Secondary HRP Antibody (#043-522-2, Biotechne) and Anti-Rabbit Secondary HRP Antibody (Protein Simple Cat# 042-206, RRID:AB_2860577). Chemiluminescence signals were quantified using the Compass software, which generated chemiluminescence spectra and lane view images. Signals were normalized to total protein (#DM-TP01, Biotechne).

2.15 | Statistical methods

Data are presented as mean ± SEM, except for survival curves. Sample sizes subjected to statistical analysis consist of at least five independent biological replicates; otherwise, the results are considered exploratory or preliminary.

For *in vitro* testing of different drug concentrations on intracellular Ca^{2+} load in primary rat neuronal cultures, each data point represents an independent neuron from a distinct well, derived from an independent embryo, across three separate experiments. For *in vitro* testing of different drug concentrations on electrophysiological parameters in primary rat neuronal cultures, each data point represents a distinct well, derived from an independent embryo, across three separate experiments. *In vitro* drug testing in HEK cell lines and iCell Cardiomyocytes² utilized three to six replicates per treatment group. For *in vitro* protocols, blinding was not feasible as experiments were conducted by an individual experimenter. Experiments with fewer than five samples were considered exploratory and were not subjected to statistical comparison due to the limited sample size. For experiments with five or more samples, normality was assessed using the Shapiro-Wilk test before further statistical analysis. Differences in CEPIAer fluorescence due to genotype in HEK cells were analysed using an unpaired t-test. Changes in cytoplasmic Ca^{2+} load in rat cortical neurons induced by H_2O_2 treatment were analyse d using a paired t-test. Changes in electrophysiological parameters of primary rat neurons over days in culture were analysed using two-way ANOVA. Post hoc tests were conducted only if F of interaction in ANOVA achieved $P < 0.05$ to identify specific differences between groups.

For the *in vivo* drug pharmacokinetics and efficacy testing experiments, data were collected in individual animals. The experimenter was blind to animal phenotype and treatment during behavioural and electrophysiological experiments. For each experiment, the normality was tested with the Shapiro-Wilks test. Changes in body weight, electrophysiological and behavioural measurements produced by treatment along time were analysed with two-way ANOVA. Post hoc tests were conducted only if F of interaction in

ANOVA achieved P < 0.05 to characterise differences among individual groups of mice. Changes in histological data produced by treatment were analysed with one-way ANOVA. Post hoc tests were conducted only if F in ANOVA achieved P < 0.05. The survival time of mice was evaluated using Kaplan–Meier analysis and Log-Rank test. Changes of gene and protein expression produced by treatment were analysed by unpaired *t*-test.

The computer-assisted analysis of the bands obtained in western blot was performed with AlphaEase FC software (Bonsai Technologies Group, S.A.). Statistical analysis was performed using SPSS (version 20, IBM, Armonk, NY, USA) and graphs were made using GraphPad Prism Software (Version 5, La Jolla, CA, USA) and Microsoft Excel. Statistical significance was set at $P < 0.05$.

2.16 | Materials

Compounds MP-001 (4-[[(3-Methoxyphenyl)thio]methyl]-1H-1,-2,3-triazole-1-acetic acid), MP-004 (4-[[(4-Methoxyphenyl)thio]methyl]-N,N-dimethyl-1H-1,2,3-triazole-1-ethanamine) and MP-010 (4-[[(4-Methoxyphenyl)sulfinyl]methyl]-N,N-dimethyl-1H-1,2,3-triazole-1-ethanamine, strategically designed to target the interaction site of FKBP12/RyR1, were synthesized by us using CuAAC 'click chemistry' methodologies. Specifically, aryl propargyl sulfides and methyl azidoglycinate were utilized for MP-001, while 2-azidoethyl-N,N-dimethylammonium hydrochloride was employed for MP-004 synthesis (Aizpurua et al., 2021; Passannante et al., 2023). Compound MP-010 was prepared by adding phthaloyl peroxide (Gan et al., 2017) to a solution of MP-004, followed by stirring at room temperature, basification with 7 N NH_3 in MeOH and evaporation under reduced pressure. The resulting crude product underwent purification through column chromatography (silica gel; eluent: CH_2C_{l2}/MeOH [7 N NH_3]). The yield of the purified white solid was 66%, with ^1H and ^{13}C NMR spectra confirming the chemical structure: ^1H NMR (400 MHz, CD_3OD) δ 7.81 (s, 1H), 7.49 (d, $J = 8.8$ Hz, 2H), 7.95 (d, $J = 8.8$ Hz, 2H), 4.51 (t, $J = 6.3$ Hz, 2H), 4.30 (dd, $J = 13.7$, 1.6 Hz, 2H), 3.86 (s, 3H), 2.82 (t, $J = 6.3$ Hz, 2H), 2.31 (s, 6H). ^{13}C NMR (101 MHz, CD_3OD) δ 164.1, 137.5, 133.5, 127.7, 126.7, 115.9, 59.5, 56.1, 53.6, 45.4. IR (cm^{-1}): 1592, 1495, 1459, 1303, 1249, 1172, 1086, 1022, 829, 524.

To obtain aqueous 10-mM stock solutions of these compounds for pharmaceutical application, the free carboxylic acid of MP-001 or the tertiary amine moiety of MP-010 was neutralized to pH = 6.8 using 2-M NaOH and 2 M HCl, respectively. These neutralized solutions were further diluted with drinking water to achieve pharmaceutically acceptable concentrations of 1 or 2 mM prior to administration.

Cell culture reagents and materials included DMEM (Thermo Fisher Scientific, Cat# 11995-065), FBS (Thermo Fisher Scientific, Cat# 16000044), poly-D-Lysine (Sigma-Aldrich, Cat# P6407), Neurobasal medium (Thermo Fisher Scientific, Cat# 21103049), B27 (Thermo Fisher Scientific, Cat# 17504044), Glutamax (Thermo Fisher Scientific, Cat# 35050061), and antibiotics (Thermo Fisher Scientific, Cat# 15240062). Polyethylenimine (PEI) (Sigma-Aldrich, Cat# P3143) was used for cell coating, and Ibidi well plates (Ibidi, Cat# 89626) were used for plating. Microelectrode array (MEA) plates (Axion Biosystems, Cat# 24-well CytoView MEA plates) were used for electrophysiological recordings. Calcium indicators Fura-2 AM (Thermo Fisher Scientific, Cat# F1200) and Fluo-8 AM (AAT Bioquest, Cat# 24181) were used for fluorescence measurements. For tissue fixation and histology, paraformaldehyde (Sigma-Aldrich, Cat# 158127) and sucrose (Sigma-Aldrich, Cat# S0389) were used. Immunohistochemical staining was performed using the VECTASTAIN® Elite ABC -HRP Kit (Vector, Cat# pk6100) and DAB solution (Vector, Cat# SK-4100). Primary antibodies used for immunostaining included Iba1 (FUJIFILM Wako Pure Chemical Corporation, Cat# 019-19741, RRID:AB_839504), GFAP (Thermo Fisher Scientific, Cat# 13-0300, RRID:AB_2532994), neurofilament 200 (NF200, Millipore, Cat# AB5539, RRID:AB_11212161), and synaptophysin (Abcam, Cat# ab32127, RRID:AB_2286949). Secondary antibodies included anti-Rat IgG biotinylated (Vector Laboratories, Cat# BA-9400, RRID:AB_2336202), anti-Rabbit IgG biotinylated (Vector Laboratories, Cat# BA-1100, RRID:AB_2336201), Alexa Fluor 594-conjugated secondary antibody (Thermo Fisher Scientific, Cat# A-11042, RRID:AB_2534099), and Alexa Fluor 488-conjugated α-bungarotoxin (Thermo Fisher Scientific, Cat# B35451, RRID:AB_2617152).

2.17 | Nomenclature of targets and ligands

Key protein targets and ligands in this article are hyperlinked to corresponding entries in the IUPHAR/BPS Guide to PHARMACOLOGY http://www.guidetopharmacology.org and are permanently archived in the Concise Guide to PHARMACOLOGY 2023/24 (Alexander, Fabbro, et al., 2023; Alexander, Mathie, et al., 2023).

3 | RESULTS

3.1 | Pharmacokinetics, target engagement and *in vitro* safety of novel FKBP12 ligands

The newly designed 4-arylthiomethyl-1-carboxyalkyl-1,2,3-triazoles were synthesized with the aim of serving as potential ligands that can concurrently bind to both the ionic and hydrophobic pockets of the FKBP12/RyR1 complex (Aizpurua et al., 2021). These compounds demonstrated *in vitro* target engagement with FKBP12 through the rapamycin-inducible FKBP/FRP binding domain protein fragment complementation assay, thereby stabilizing cytosolic Ca^{2+} levels in human myotubes under nitro-oxidative stress (Aizpurua et al., 2021). Within this class of compounds, MP-001 (Figure 1a) demonstrated superior binding affinity to FKBP12 and elicited co-localization of FKBP12/RyR1 in human myotubes under nitro-oxidative stress conditions, as reported before (Aizpurua et al., 2021). MP-001 not only attenuated Ca^{2+} ER leakage through the RyR induced by nitro-oxidative stress but also demonstrated the capacity to rectify the

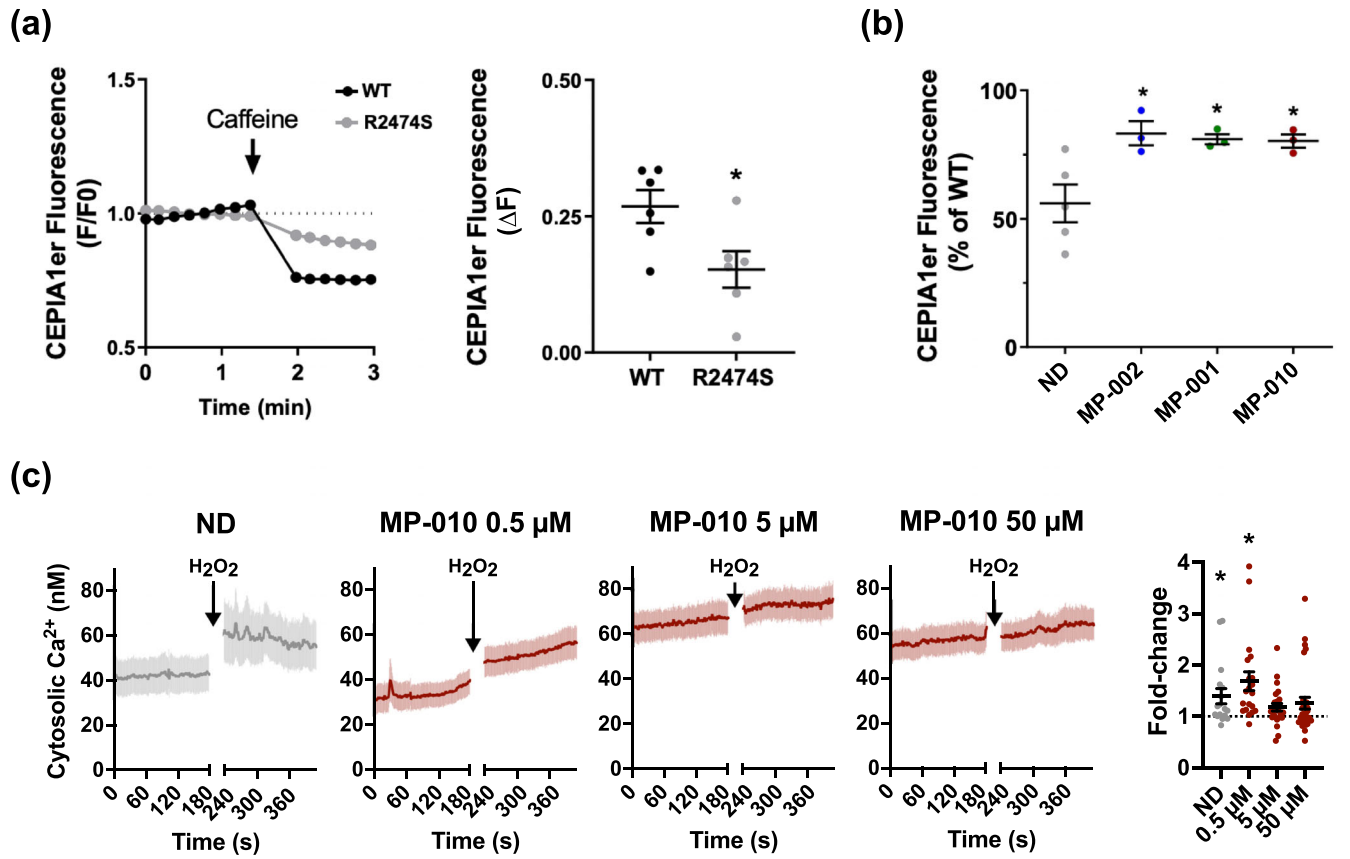

FIGURE 1 Chemical structure of RyR stabilizers and concentration-time profiles in mice following a single Oral bolus of MP-010 or MP-001 at a dose of 30 mg·kg^{-1}. (a) Chemical structures of FKBP12 ligands MP-001, MP-004 and MP-010. Compound MP-001 restored cytosolic calcium homeostasis in myotubes but show limited BBB permeability (see Figure 1a–c). Modification to MP-004 improved BBB permeability, although the compound displayed too short serum half-time for systemic administration. Finally, the chemical incorporation of the sulfoxide function into MP-010 provided favourable pharmacokinetic parameters for development. (b–d) control mice were administered a single dose of MP-010 or MP-001 at 30 mg·kg^{-1} by oral gavage and their concentrations were assessed at 2, 4, 6 and 18 h post-dosing in the plasma (b), skeletal muscle (c) and brain (d). (d) The calculated mean brain-to-serum (Cb:Cs) ratio for MP-010 exhibited values above the threshold (Cb:Cs > 0.04, dashed line), suggesting penetrability to the brain. The presented concentrations and values are the mean ± S.E.M. with n = 3; these data are designated as exploratory due to the low sample size and thus no statistical comparisons were made.

heightened susceptibility to spontaneous Ca^{2+} release observed in conditions of ER Ca^{2+} overload resulting from the RyR2-R2474S mutation, which disrupts the interaction with the FKBP12.6 subunit (Lehnart et al., 2008). This manifestation is evidenced by the increased Ca^{2+} content released upon stimulation with caffeine.

Polar group exchange from carboxylic acid to N,N-dimethylamino moiety yielded compound MP-004 (Figure 1a) with improved blood–brain–brain barrier (BBB) permeability. However, MP-004 exhibits very rapid metabolism, which results in low circulating levels, making it unsuitable for chronic treatment of the central nervous system. Concretely, MP-004 displayed a C_{max} of 5.1 ± 2.4 ng·ml^{-1} with an inappreciable half-life in serum after an oral dosing of 30 mg·kg^{-1} (data not shown).

Subsequently, for chronic treatment in the SOD1^{G93A} mouse model, we selected compound MP-010 (Figure 1a) as an improved version of MP-004, incorporating a sulfoxide functional group to enhance its pharmacokinetic properties. Although MP-010 is likely a substrate of **P-glycoprotein (ABCB1)**, which could slightly affect its oral bioavailability, it exhibited high permeability across the intestinal epithelium in a Caco-2 assay comparable to well-absorbed drugs like metoprolol (Table 1). In this sense, an exploratory pharmacokinetic analysis showed that MP-010 had favourable oral absorption *in vivo*, with a mean C_{max} of 1144.4 ± 397.2 ng·ml^{-1} and a half-life of 3.0 h in serum (Figure 1b), a C_{max} of 1173.1 ± 279.6 ng·g^{-1} and a half-life of 2.5 h in muscle (Figure 1c) and a C_{max} of 340.8 ± 166.9 ng·g^{-1} and a half-life of 3.7 h in the brain after a dosing of 30 mg·kg^{-1} (Figure 1d). The brain-to-serum concentration ratio (Cb:Cs) of MP-010 was greater than 0.04, even after 18 h following dosing (Figure 1d). This value is the threshold at which a molecule is commonly considered to be 'brain penetrant', as blood brain volume approximates 4% of total brain volume (Shaffer, 2010). The low plasma protein binding profile of MP-010 (<10%; Table S2) may facilitate its penetration into the CNS, while also offering benefits such as a reduced risk of drug–drug interactions and enhanced renal clearance.

With respect to the stabilizing properties of RyR, exploratory experiments suggest that both compounds MP-004 and MP-010 are

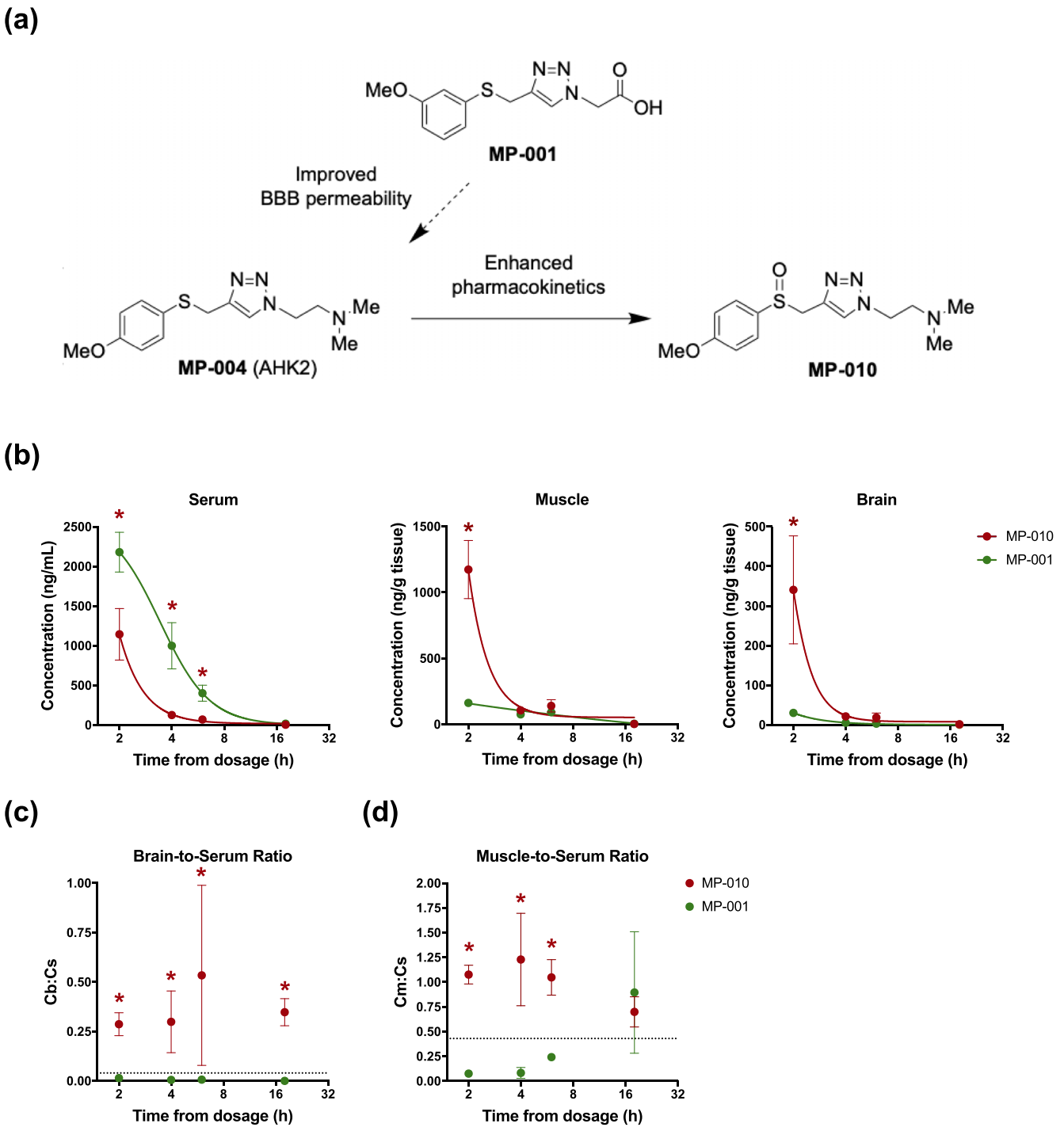

FIGURE 2 Modulation of cytosolic Ca^{2+} by compound MP-010. (a) Caffeine-induced endoplasmic reticulum (ER) Ca^{2+} release is significantly reduced in HEK293 cells expressing the mutant R2474S-RyR2 compared to WT cells. This suggests that Ca^{2+} stores in the ER are depleted due to the continuous leakage of mutant RyR2 channels. The presented values are the mean ± S.E.M. with n = 6 per group. Statistical differences were calculated with unpaired *t*-test. **P* < 0.05. (b) Pretreatment with MP compounds increase caffeine-induced ER Ca^{2+} release in RyR2 HEK mutants, suggesting that RyR2 leakage is mitigated. Cells were pretreated or not for 1 h with MP compounds. The 10-mM caffeine was used to empty ER stores. ND (non-drug) refers to the effect of caffeine in non-treated HEK293 expressing RyR2-R2474S. Assays were performed in triplicates. The presented values are the mean ± S.E.M. with n = 5, 3, 3 and 3. These data are designated as exploratory due to the low sample size and thus no statistical comparisons were made. (c) Hydrogen peroxide (H_2O_2; 100 μM) treatment of primary rat cortical neurons significantly increased cytosolic Ca^{2+} concentration compared to non-drug (ND) controls. However, increasing concentrations of MP-010 attenuated the H_2O_2- induced rise in Ca^{2+}. The right panel shows the quantification of the fold-change determined in a pooled dataset from three independent experiments. The presented values are the mean ± S.E.M. with n = 17, 21, 25 and 30. Statistical differences were calculated using paired *t*-test: **P* < 0.05 post-H_2O_2 versus basal line.

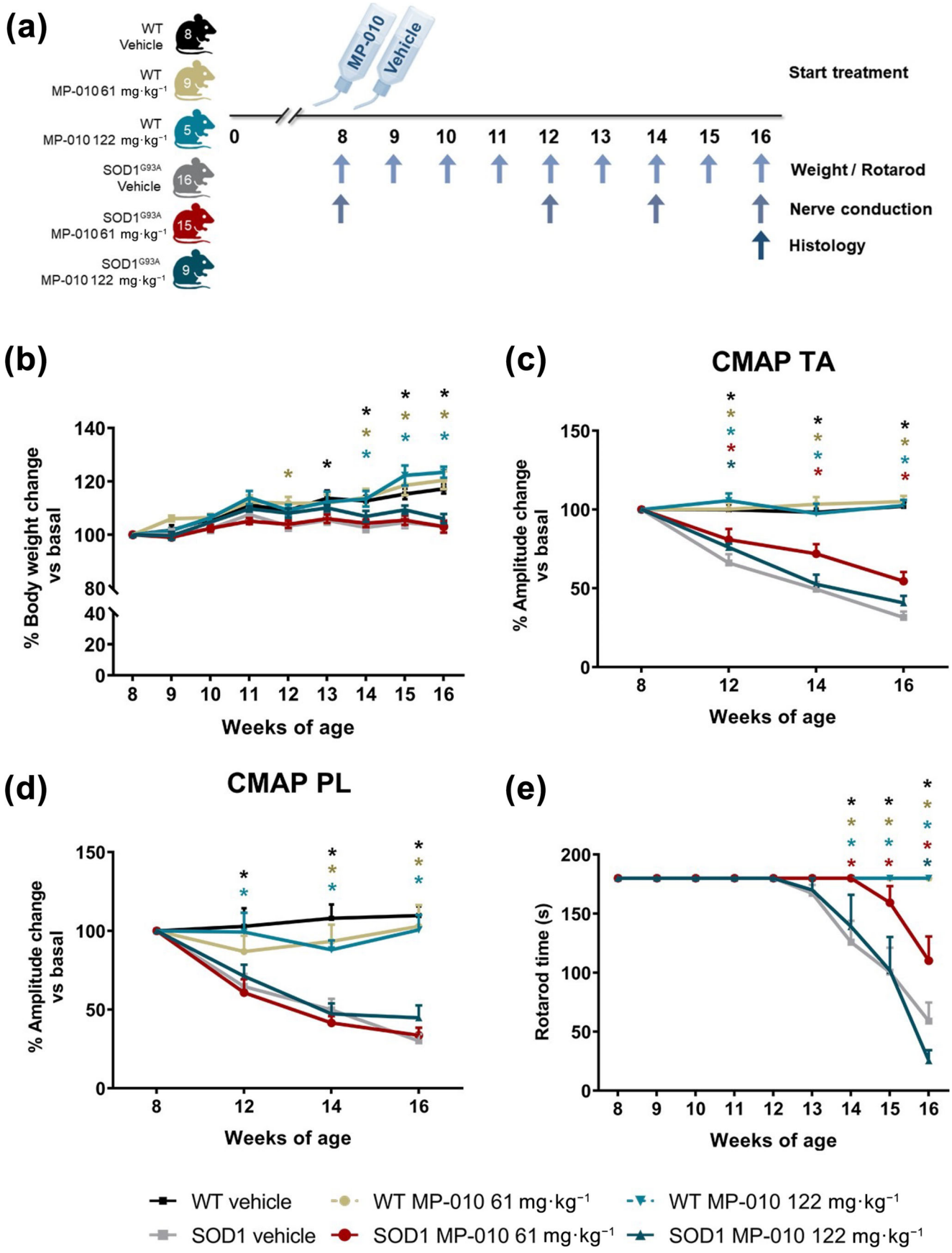

FIGURE 3 Legend on next page.

able to rectify the Ca^{2+} ER leak caused by the RyR2-R2474S mutation in HEK cells, as evidenced by the increased Ca^{2+} content released upon stimulation with caffeine (Figure 2a,b). Moreover, in primary cortical neurons from rats, treatment with MP-010 significantly reduced the intracellular Ca^{2+} elevation induced by 100 μM H_2O_2, whose effects on the oxidation of RyR channels and subsequent Ca^{2+} leakage are well established (Figure 2c). Moreover, at all tested *in vitro* concentrations, MP-010 had no effect on the activity of the SERCA pump, another ER channel known to regulate cytosolic Ca^{2+} levels. This was confirmed by the unchanged decay time (tau) of spontaneous Ca^{2+} transients, although a slight upward trend (indicative of SERCA pump inhibition) was observed at the highest concentration of 50 μM (Figure 1). This suggests that MP-010 exhibits much greater selectivity for RyR channels.

In evaluating the neurotoxicity of MP-010, none of the tested concentrations (0.5, 5 and 50 μM) over a 16-day continuous exposure period led to a significant decrease in the mean firing rate, neuronal burst frequency or synchrony index, which are markers of neuronal function, synaptic integrity and network activity in primary rat cortical neurons (Figure S2a). Notably, the intermediate concentration of 5 μM resulted in a significant increase in both mean firing rate and network burst frequency, suggesting a potential enhancement of synaptic and neuronal function at this concentration. Additionally, we investigated whether MP-010 could produce neurotoxic metabolites in the liver. In mouse liver microsomes, both MP-010 and four metabolites (M1–M4) were detected, with M1 and M2 identified as the major metabolites, contributing 10.5% and 8.2% of the total drug-related components, respectively (Figure S3a,b). In human liver microsomes, three of the four metabolites identified in mouse (M1, M2 and M4) were observed, with M1 and M4 accounting for 9.5% and 10.9% of the total drug-related components (Figure S3a,b). The metabolites M1 and M4 were classified as demethylated, while M2 and M3 were identified as mono-oxidized metabolites (Figure S3c). Importantly, the parent compound MP-010 constituted a substantial proportion of the total drug-related components, representing 73.7% in mouse microsomes and 72.8% in human microsomes after the incubation period. Furthermore, MP-010 showed no inhibition of major drug-metabolizing cytochrome P450 enzymes (Table S3). Notably, none of the hepatic metabolites, at a concentration of 10 μM and under continuous exposure for 16 days, produced neurotoxic effects, as they did not induce any major changes in the electrophysiological parameters of primary cortical neurons (Figure S2b).

Given the potential modulatory mechanism of the RyR channels by the compound MP-010 and considering the likely adverse effects on other organs where Ca^{2+} dynamics are tightly regulated, such as the heart, we aimed to investigate any cardiotoxicity that this compound might exert on cardiomyocytes. To assess this, we exposed induced pluripotent stem cell-derived cardiomyocytes to concentrations of MP-010 up to 20 mM for 20 h. Our exploratory results showed that concentrations below 1 mM did not appear to affect the viability of the cardiomyocytes. The determined *in vitro* cardiotoxic concentration 50 was found to be 8.26 mM, which is several orders of magnitude higher than expected plasma levels (Figure S2c).

According to these results, MP-010 possesses a favourable safety and pharmacokinetic profile, making it a suitable candidate for preclinical evaluation of its neuroprotective potential in ALS. We hypothesized that modulating intracellular Ca^{2+} levels by facilitating FKBP12-RyR interactions could contribute to this effect. Additionally, we sought to evaluate another compound with comparable *in vivo* stability to MP-010 but with a more limited tissue distribution. Our aim was to determine that any positive effects of MP-010 are attributable to its mechanisms of action within the CNS. Based on this assumption, we chose MP-001 as an alternative compound, with a C_{max} and half-life of 2179.8 ± 305.9 ng·ml^{-1} and 2.5 h in serum (Figure 1b), 163.0 ± 22.1 ng·g^{-1} and 2.5 h in muscle (Figure 1c) and 30.3 ± 5.6 ng·g^{-1} and 1.2 h in the brain (Figure 1d), respectively. Its brain-to-serum concentration ratio ratio was found to be less than 0.04 (Figure 1d).

3.2 | Evaluating the efficacy of compound MP-010 in alleviating neuromuscular deficits in SOD1^{G93A} mice

To test our hypothesis that modulating the FKBP12-RyR interaction could mitigate excessive intracellular Ca^{2+} overload in ALS motor neurones, we first validated this target in the SOD1^{G93A} mouse model, which is widely recognized for studying ALS pathophysiology. This validation was essential to ensure that MP-010, our compound designed to modulate this interaction, effectively targets a relevant mechanism in the disease. Immunoblotting assays were performed to quantify FKBP12.6 and **RyR2** protein levels in the spinal cord of SOD1^{G93A} mice. A significant reduction in FKBP12.6 protein expression ($P = 0.0312$) was observed in SOD1^{G93A} mice (Figure S4a), similar to findings in the spinal cords of ALS patients (Kihira

FIGURE 3 Improvement of motor function in superoxide dismutase 1 (SOD1)^{G93A} mice upon MP-010 treatment. (a) Schematic diagram of the experimental design for the trial whose data are shown in this figure and Figure 3. (b) Plot of the percentage of body weight for the different mice groups during the follow-up period. Body weight results are expressed as a percentage relative to baseline values for each mouse. (c,d) Electrophysiological tests illustrating the preservation of compound muscle action potentials (CMAP) amplitude in the tibialis anterior (TA) muscle but not in the plantar interosseous (PL) muscle at 16 weeks of age. Amplitude values of CMAP are presented as a percentage relative to the baseline value for each mouse. (e) Graph depicting the impact of different MP-010 treatments on functional outcome in the rotarod test. The presented values are the mean ± SEM. Animals per group: WT vehicle, n = 8; WT MP-010 61 mg·kg^{-1}, n = 9, WT MP-010122 mg·kg^{-1}, n = 5, SOD1^{G93A} vehicle, n = 16; SOD1^{G93A} MP-010 61 mg·kg^{-1}, n = 15; SOD1^{G93A} MP-010 122 mg·kg^{-1}, n = 9. Statistical differences were calculated with two-way ANOVA with Bonferroni's multiple comparisons test. *$P < 0.05$ compared to the SOD1^{G93A} vehicle group. Each coloured * represents the comparison between each group (defined by colours on panel a) and the SOD^{G93A} vehicle group (grey). Gender-stratified analysis are shown in Figure S5.

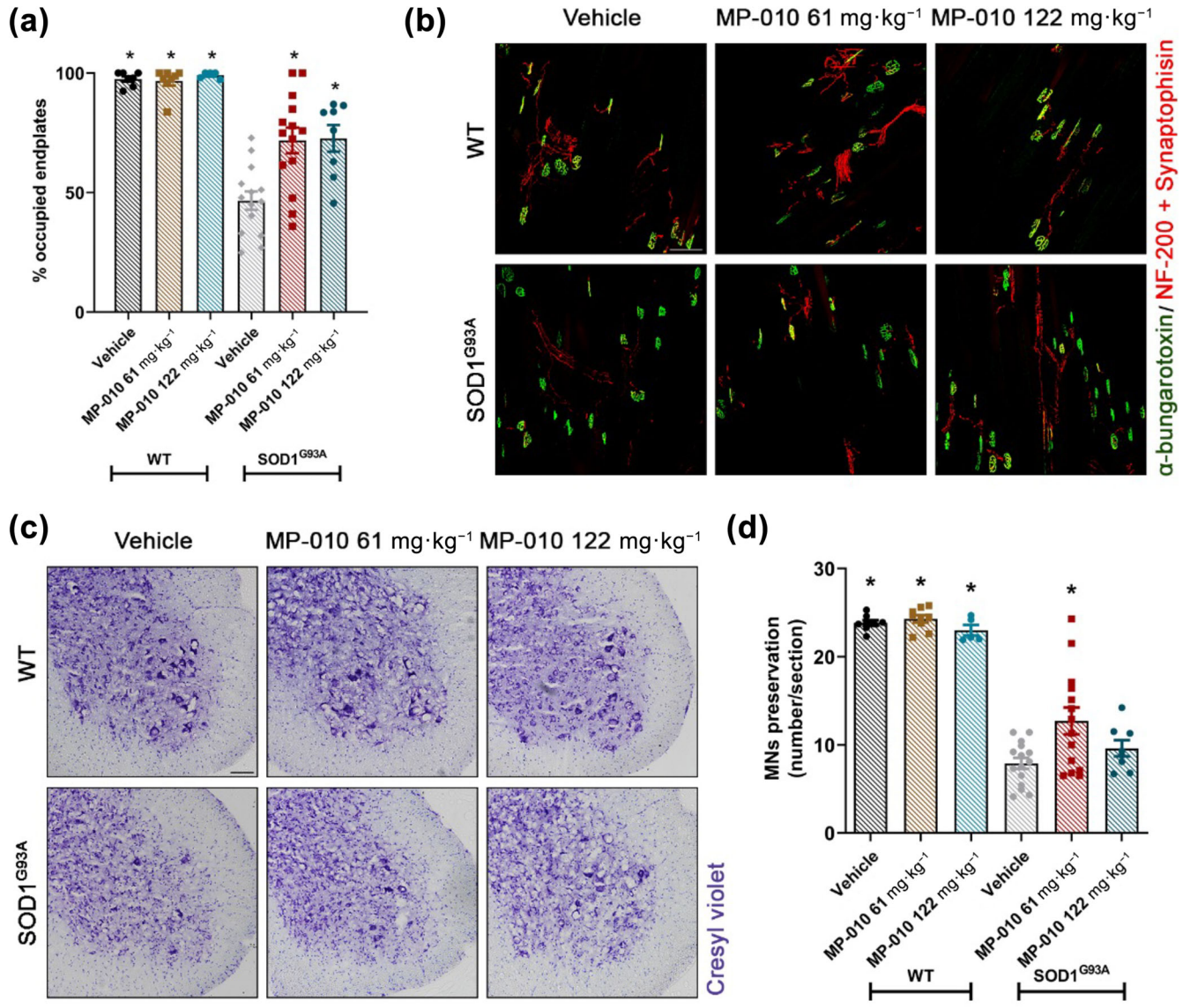

FIGURE 4 Preservation of neuromuscular junction (NMJ) innervation and spinal motor neurones in superoxide dismutase 1 (SOD1)^{G93A} mice upon MP-010 treatment. (a) Plot illustrating the percentage of NMJ innervated (overlap of signals) in the different mouse groups. (b) Representative confocal images of NMJ in tibialis anterior (TA) muscles of mice at 16 weeks of age, presented as maximum projections generated from 1.3 μm z projections. Immunolabelling against **α-bungarotoxin** (nicotine receptor, in green), neurofilament 200 + synaptophysin (synapse, in red) was performed to assess NMJ innervation. Scale bar: 100 μm. (c) Representative images of lumbar spinal sections depicting motor neurones stained with cresyl violet from mice at 16 weeks of age. Scale bar: 100 μm. (d) Plot showing the number of surviving spinal motor neurones (mean number of motor neurones per section ± SEM) in L4-L5 segments at 16 weeks of age in the different mouse groups. The presented values are the mean ± SEM. Animals per group:- WT vehicle, n = 8; WT MP-010 61 mg·kg^{-1}, n = 9, WT MP-010122 mg·kg^{-1}, n = 5, SOD1^{G93A} vehicle, n = 16; SOD1^{G93A} MP-010 61 mg·kg^{-1}, n = 15; SOD1^{G93A} MP-010 122 mg·kg^{-1}, n = 9. Statistical differences were calculated with one-way ANOVA with Bonferroni multiple comparisons test. *P < 0.05 compared to the SOD1^{G93A} vehicle group. Gender-stratified analysis are shown in Figure S5.

et al., 2005). Notably, this reduction occurs even before symptom onset, at postnatal Day 60, in the mouse model. Additionally, a slight increase in RyR2 protein expression was also observed in this group (Figure S4b).

In the first phase of our study, we examined the potential of MP-010 to ameliorate motor impairments and neuromuscular dysfunction in SOD1^{G93A} transgenic mice. To this end, the animals were given two different doses of MP-010 (61 and 122 mg·kg^{-1}) (Figure 3a). Remarkably, the chronic administration of MP-010 at both doses examined did not result in any discernible differences in body weight between treated and vehicle groups of WT or SOD1^{G93A} mice (Figure 3b). A notable increase in body weight was noted in the WT groups compared to the SOD1^{G93A} vehicle-treated group, particularly at the 12- to 16-week time points (Figure 3b). This emphasizes the expected divergence in body weight trajectories between the WT and SOD1^{G93A} cohorts throughout the study.

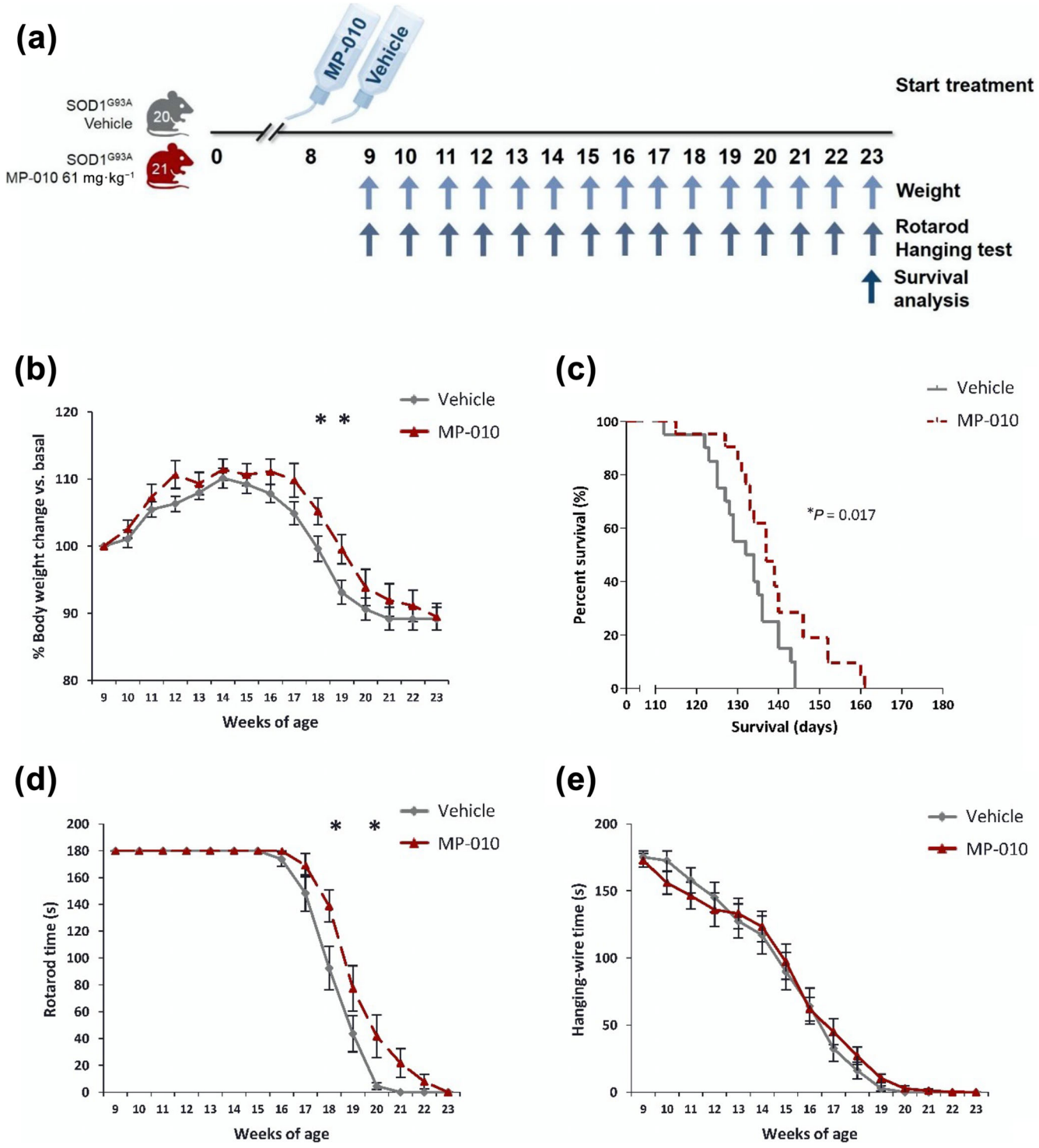

FIGURE 5 Enhanced survival and amelioration of motor symptoms in superoxide dismutase 1 (SOD1)^{G93A} mice treated with MP-010. (a) Schematic diagram of the experimental design of this trial. (b) Plot illustrating the percentage of body weight in female and male mice across different groups during the follow-up period. Body weight results are expressed as a percentage relative to baseline values for each mouse. (c) Survival curves indicate that treated mice exhibited a longer lifespan compared to untreated counterparts, as determined by the log-rank (Mantel–Cox) test. *$P = 0.017$ compared to the SOD1^{G93A} vehicle group. (d) MP-010 treatment resulted in an improvement in motor coordination, as assessed by the rotarod test. (e) MP-010 treatment did not lead to improved motor strength, as evaluated in the hanging-wire test. In all datasets, group sizes are: SOD1^{G93A} vehicle, n = 20; SOD1^{G93A} MP-010 61 mg·kg^{-1}, n = 21. With the exception of the survival curves, the presented values are the mean ± SEM and statistical differences were calculated with two-way ANOVA with Bonferroni's multiple comparisons test. *$P < 0.05$ compared to the SOD1^{G93A} vehicle group. Gender-stratified analysis are shown in Figure S7.

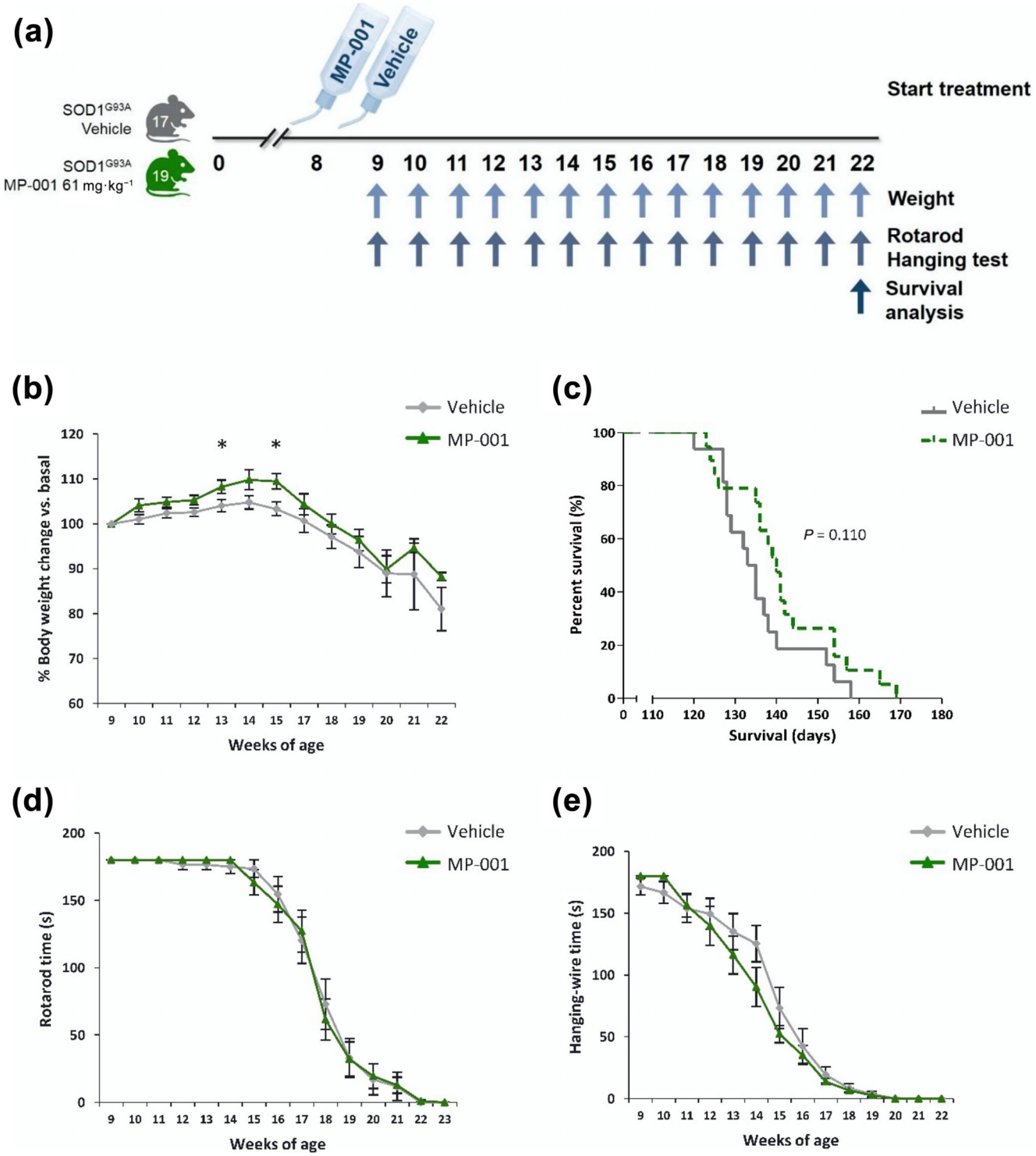

FIGURE 6 Marginal extension of survival and attenuation of weight loss in superoxide dismutase 1 (SOD1) ^{G93A} mice upon MP-001 administration. (a) Schematic diagram of the experimental design for the trial to test MP-001. (b) Mice treated with MP-001 exhibited reduced weight loss at 13–15 weeks of age. (c) Treated mice displayed a slightly longer lifespan compared to untreated counterparts, but the differences were not statistically significant, as determined by the Log-rank (Mantel–Cox) test. (d) The treated and control animals demonstrated comparable results concerning motor coordination in the rotarod test. (e) SOD1^{G93A} mice under treatment did not exhibit an improvement in motor strength, as assessed in the hanging-wire test. In all datasets, group sizes are: SOD1^{G93A} vehicle, n = 17; SOD1^{G93A} MP-010 61 mg·kg^{-1}, n = 19. With the exception of the survival curves, the presented values are the mean ± SEM and statistical differences were calculated with two-way ANOVA with Bonferroni's multiple comparisons test. *P < 0.05 compared to the SOD1^{G93A} vehicle group. Gender-stratified analysis are shown in Figure S8.

Electrophysiological assessments during the follow-up revealed that MP-010 treatment at a dose of 61 mg·kg^{-1} prevented the decline of the compound muscle action potential amplitude compared to untreated SOD1^{G93A} mice (Figure 3c). Notably, at early (12 weeks), intermediate (14 weeks) and advanced (16 weeks) disease stages of the disease, MP-010 at 61 mg·kg^{-1} exerted significant effects on the compound muscle action potential amplitude preservation in the tibialis anterior muscle of SOD1^{G93A} mice (Figure 3c). This improvement in motor function was observed in both male and female mice when analysed separately (Figure S5a). In contrast, mice treated with the 122-mg·kg^{-1} dose did not manifest a substantial improvement compared to the vehicle-treated group (Figure 3c). In the plantar interossei muscle there were no significant improvements with any of the doses of MP-010 in the treated SOD1^{G93A} mice (Figure 3d).

The rotarod test was used to assess locomotion and coordination, and to pinpoint the initiation of the symptomatic phase of the disease. The administration of MP-010 at the dose of 61 mg·kg^{-1} caused a significant improvement in rotarod performance at an advanced disease stage (14–16 weeks of age in SOD1^{G93A} mice) (Figure 3e), delaying the onset of motor impairment by 2 weeks compared to untreated animals (13 weeks). In contrast, in accordance with the compound muscle action potential data, there was no change in rotarod performance between SOD1^{G93A} mice treated with 122 mg·kg^{-1} and vehicle control. The beneficial effects of the 61-mg·kg^{-1} regime were indicative of a deceleration in the progression of the disease, highlighting the potential therapeutic impact of MP-010 on mitigating motor deficits in SOD1^{G93A} mice.

At the end of the functional follow-up (16 weeks of age), a significant increase in the number of innervated NMJ within the tibialis anterior muscle in SOD1^{G93A} mice receiving MP-010 treatment at both doses was observed compared to the vehicle-treated groups (Figure 4a,b). This finding supports the observed preservation of the compound muscle action potential amplitude in nerve conduction tests. Upon stratifying the analysis by sex, a more pronounced enhancement in neuromuscular junction (NMJ) innervation was observed in males, the increase being significant. Conversely, females demonstrated a trend towards improvement, potentially limited by the sample size (Figure S5b).

3.3 | Evaluating the efficacy of compound MP-010 in preserving motor neurone loss in SOD1^{G93A} mice

At the end of the functional follow-up, spinal cords wer harvested for histological studies. The quantification of alpha motor neurones in the ventral horn of spinal cord sections stained with cresyl violet showed that untreated control SOD1^{G93A} mice experienced a loss of over 60% of motor neurones compared to WT mice at 16 weeks of age (Figure 4c,d). This finding was consistently observed in both sexes even when analysed separately (Figure S5c). The administration of MP-010 at 61 mg·kg^{-1} significantly increased the number of surviving motor neurones in SOD1^{G93A} mice, whereas the dose of 122 mg·kg^{-1} MP-010 did not mitigate motor neurone loss (Figure 4c,d). When examining the treatment effects on motor neurone survival by sex, males exhibited again a more notable protective effect, evidenced by a significant increase. However, females displayed a suggestive trend of improvement, possibly constrained by the sample size (Figure S5c).

The glial response to the damage triggered by motor neurone death was not reversed by treatment, as neither the levels of the astrocytic reactivity marker GFAP nor the microglial reactivity marker Iba1 were reduced at any dose of MP-010 (Figure S6).

3.4 | Evaluating the efficacy of compound MP-010 in lifespan in SOD1^{G93A} mice

After observing that MP-010 treatment confers motor and electrophysiological benefits, leading to reduced motor neurone loss, a second trial in SOD1^{G93A} mice was conducted to investigate its potential to extend survival, particularly at the dosage of 61 mg·kg^{-1} (Figure 5a). Our observations revealed that MP-010-treated animals exhibited reduced weight loss compared to vehicle-treated controls, with significant differences becoming apparent at 18–19 weeks of age (Figure 5b). The results obtained in the survival study indicated that MP-010 delayed mortality by approximately 7 days, extending the average lifespan from 132 ± 8.35 days in vehicle-treated SOD1^{G93A} mice to 139 ± 10.92 days in MP-010-treated mice (Figure 5c). These treatment effects were more pronounced in female SOD1^{G93A} mice (Figure S7a,b).

Analysing the outcomes of the behavioural tests, we again observed that MP-010-treated SOD1^{G93A} mice at the dose of 61 mg·kg^{-1} demonstrated enhanced rotarod performance at advanced stages compared to vehicle-treated counterparts (Figure 5d). Motor strength, assessed in the hanging-wire test, revealed no significant differences between the two groups of animals (Figure 5e). When the analysis was divided by sex, the improvement in motor function and lifespan was observed to be more prominent in female mice (Figure S7c,d).

3.5 | Evaluating the efficacy of compound MP-001 in survival, motor function and muscular markers in SOD1^{G93A} mice

We also investigated on SOD1^{G93A} mice the therapeutic potential of the compound MP-001 (Figure 6a), characterized by limited or negligible CNS availability (Figure 1), thereby confining its mechanism of action more likely to peripheral tissues. The body weight of all animals was monitored weekly from 8 weeks of age until 22 weeks. We observed reduced weight loss in the treated animals, with significant differences at the 13th and 15th weeks of age (Figure 6d). However, as shown in the survival analysis, MP-001 treatment did not significantly extend the survival of SOD1^{G93A} mice (Figure 6c). Regarding the results obtained in the motor tests, no discernible improvement was observed in the SOD1^{G93A} mice treated with MP-001

(Figure 6d,e). When the analysis was divided by sex, no improvement in motor function, lifespan or body weight was observed in either sex (Figure S8a–d).

4 | DISCUSSION AND CONCLUSIONS

Our investigation centred on modulating RyR activity, specifically through a novel class of triazole molecules known as MP compounds that act as FKBP12 ligands (Aizpurua et al., 2021). The primary focus of our study was on MP-010, a RyR stabilizer with favourable pharmacokinetics and CNS permeability. Our results in SOD1^{G93A} mice, a widely accepted ALS model, demonstrated significant benefits following MP-010 administration. Notably, increased survival, protection against motor neurone loss, muscle denervation and enhanced neuromuscular function were observed, highlighting the potential of MP-010 as a therapeutic intervention for ALS. The robustness of our findings is emphasized by the complementary studies performed in two distinct colonies of SOD1^{G93A} mice with a mixed hybrid B6SJL genetic background, across two independent laboratories. This complementation is particularly noteworthy considering the potential genetic drift that hybrid ALS SOD1 colonies may undergo among different research labs, leading to variability in disease onset or symptom severity (Heiman-Patterson et al., 2005; Mancuso et al., 2012). This potential confounding factor makes the replication of our findings in two independent laboratories even more significant. Remarkably, despite differing ages of motor symptom onset between the two colonies (14 weeks in one laboratory and 17 weeks in the other), MP-010 demonstrated beneficial effects in both settings at the dose of 61 mg·kg^{-1}. The compound exhibited remarkable tolerability and appeared devoid of apparent toxicity even at high doses. Doubling the dose did not induce a change in body weight, a recognized clinical symptom of pharmacological toxicity. Nevertheless, the compound therapeutic efficacy was compromised at this higher dose. This unexpected loss of efficacy could be attributed to off-target effects. These unintended interactions with non-target proteins could be interfering with the compound's ability to reach its intended target and exert its therapeutic effects. Further investigations are warranted to identify and characterize specific off-target mechanisms, enabling the development of strategies to mitigate them and optimize the compound's efficacy.

As previously mentioned cytosolic Ca^{2+} overload assumes particular importance in the vulnerability of spinal motor neurones subjected to ALS toxicity (Dekkers et al., 2004; Ho et al., 1996), and deficient Ca^{2+} handling from ER and mitochondrial stores has emerged as a key player in the pathogenesis of ALS. This sets the stage for a positive feedback loop that amplifies pathological Ca^{2+} overload, intensifying the neurodegenerative processes associated with the disease (Leal & Gomes, 2015; Tadic et al., 2014). Mutations in genes such as *SIGMA1R* and *VAPB*, identified in ALS patients, underscore the significance of ER and mitochondrial proteins in Ca^{2+} homeostasis (De Vos et al., 2012; Bernard-Marissal et al., 2015). In the context of the present study, the rationale for targeting RyR stemmed from its central role in Ca^{2+}-induced Ca^{2+} release from the ER, aiming to prevent excessive cytosolic Ca^{2+} accumulation, especially in the most vulnerable motor neurones associated with ALS. The outcomes of the current study, demonstrating the therapeutic benefits of a drug promoting the interaction between RyR and its endogenous ligand FKBP12 in the SOD1^{G93A} mouse model of ALS, are in accordance with earlier research that has emphasized reductions in FKBP12 in the context of ALS (Kihira et al., 2005). Also, in the SOD1^{G93A} mouse various alternative strategies to reduce the Ca^{2+} burden on motor neurones have been successfully implemented. These strategies include the application of the AMPA receptor antagonist **talampanel** (Paizs et al., 2011) and sigma non-opioid intracellular receptor 1 (SIGMA1R) agonists (Gaja-Capdevila et al., 2021; Mancuso et al., 2011), both exerting their effects through the modulation of extracellular Ca^{2+} influx to cytosol.

The dysregulation of RyR signalling emerges as a fundamental contributor to the pathogenesis of various neurodegenerative disorders, notably Alzheimer's disease (AD). Specifically, RyRs have been demonstrated to interact with **amyloid-beta (Aβ) peptide**, a protein known to play a pivotal role in Alzheimer's disease development. The binding of Aβ to RyRs can modulate their function, resulting in heightened Ca^{2+} release from the ER, subsequently leading to excitotoxicity, neuronal death and cognitive deficits (Lacampagne et al., 2017; Liu et al., 2012; Yao et al., 2020, 2022). Although our investigation cannot definitively ascertain the existence of Ca^{2+} leakage through RyR in ALS motor neurones or whether this pathological phenomenon is replicated in the SOD1^{G93A} mouse model, the administration of the compound MP-010 emphasizes the potential therapeutic significance of targeting FKBP12 to safeguard the RyR-dependent proper release of Ca^{2+} and alleviate the downstream effects of disrupted Ca2 + homeostasis. This approach offers a targeted intervention for ALS. However, while it is important to note that an aberrant increase in RyR-mediated Ca^{2+} release can contribute to disrupting neuronal homeostasis, triggering excitotoxicity, conversely, diminished RyR function may compromise the crucial Ca^{2+} signalling required for proper neuronal operation. This impairment might lead to a breakdown in synaptic transmission and plasticity, potentially contributing to the manifestation of motor deficits in individuals with ALS. Consequently, inhibiting RyR under this premise may not be a plausible strategy for treating neurons susceptible to ALS. Indeed, prior research utilizing dantrolene, an **RyR1** inhibitor clinically used to treat malignant hyperthermia, failed to demonstrate significant improvements when administered to the SOD1^{G93A} mouse model (Staats et al., 2012), confirming the inadequacy of RyR inhibition as a therapeutic avenue. In contrast, compounds exhibiting RyR-stabilizing activity, previously recognized under the nomenclature 'rycals' (Fauconnier et al., 2010), adopt a distinct approach by modulating RyR channel opening. These compounds achieve this modulation by facilitating the interaction between the topoisomerase FKBP12 and RyR, particularly in pathological scenarios characterized by persistent Ca^{2+} leakage (Fauconnier et al., 2010). Thus, the strategic targeting of RyR modulation through rycal compounds offers a more nuanced and potentially effective therapeutic strategy compared to direct inhibition.

Comparative analysis with MP-001, another compound characterized by limited CNS availability, provides additional insights. The

lack of MP-001 effect underscore the significance of targeting Ca^{2+} homeostasis at the CNS level to achieve therapeutic efficacy. Thus, it dismisses the possibility that the therapeutic effects could be mediated by the modulation of Ca^{2+} dynamics in cells of the innate immune system. It is crucial to consider this aspect, especially given that immune cells heavily rely on Ca^{2+}-dependent processes and tightly regulated Ca^{2+} homeostasis (Peters & Raghavan, 2011), and that the innate immune response appears to play an active role in the pathophysiology of ALS and the $SOD1^{G93A}$ mouse model (Komine et al., 2018; Nguyen et al., 2004).

While our study presents promising results, several avenues for future research emerge. Elucidating the molecular mechanisms underlying the observed effects of MP-010, particularly its impact on Ca^{2+} dynamics and neuronal survival, is critical for a comprehensive understanding of ALS pathology. Additionally, considerations of toxicity, dosage optimization and potential side effects are paramount before translating these findings into clinical trials. In conclusion, our study contributes to the evolving landscape of ALS research by highlighting the therapeutic potential of targeting intracellular Ca^{2+} dynamics through the modulation of RyR activity. MP-010, with its favourable preclinical outcomes, offers a promising avenue for further exploration and potential clinical development.

AUTHOR CONTRIBUTIONS

Laura Moreno-Martinez: Formal analysis (equal); investigation (equal); methodology (equal); writing—original draft (supporting). **Núria Gaja-Capdevila:** Formal analysis (equal); investigation (equal); methodology (equal); writing—original draft (supporting). **Laura Mosqueira-Martín:** Formal analysis (equal); investigation (equal); methodology (equal); writing—original draft (supporting). **Mireia Herrando-Grabulosa:** Investigation (equal); methodology (equal). **Laura Rodriguez-Gomez:** Formal analysis (equal); investigation (equal); methodology (equal). **Klaudia Gonzalez-Imaz:** Formal analysis (equal); investigation (equal); writing—original draft (supporting). **Ana C. Calvo:** Investigation (equal). **Maialen Sagartzazu-Aizpurua:** Resources (equal). **Leticia Moreno-García:** Investigation (equal). **Jose Manuel Fuentes:** Funding acquisition (equal); methodology (equal). **Abraham Acevedo-Arozena:** Funding acquisition (equal); investigation (equal); methodology (equal). **Jesús María Aizpurua:** Methodology (equal); resources (equal). **José Ignacio Miranda:** Methodology (equal); resources (equal). **Adolfo López de Munain:** Conceptualization (equal); funding acquisition (equal). **Ainara Vallejo-Illarramendi:** Funding acquisition (equal); methodology (equal). **Rosario Osta:** Funding acquisition (equal); methodology (equal); project administration (supporting); supervision (equal). **Xavier Navarro:** Funding acquisition (equal); methodology (equal); project administration (supporting); supervision (equal). **Francisco Javier Gil-Bea:** Conceptualization (equal); funding acquisition (equal); project administration (lead); supervision (equal); writing—original draft (equal).

ACKNOWLEDGEMENTS

Dr. Takashi Sakurai is gratefully acknowledged for his generous gift of HEK293 cells stably and inducibly expressing mutant and WT forms of RyR2 and co-expressing R-CEPIA1er, which were instrumental in the successful completion of this work. The authors thank for technical and human support provided by Mª Carmen Sampedro from SGIker of UPV/EHU and European funding (ERDF and ESF), and by Neus Hernández, Mónica Espejo and Jessica Jaramillo from the UAB for their excellent technical support.

CONFLICT OF INTEREST STATEMENT

F. J. G.-B., A. V. I., J. M. A. and A. L. M have equity ownership in Miramoon Pharma S.L., which is developing novel triazole molecules related to the research being reported. The terms of this arrangement have been reviewed and approved by the University of the Basque Country and BIOEF.

DATA AVAILABILITY STATEMENT

The data that support the findings of this study are available from the corresponding author upon reasonable request. All animal experimental procedures were approved by the Ethics Committee of the Universitat Autònoma de Barcelona (CEEAH-UAB: 2969 and 4273) and by the Ethic Committee for Animal Experiments from the University of Zaragoza (PI45/18, PI15/21, PI51/21 and PI02/23).

DECLARATION OF TRANSPARENCY AND SCIENTIFIC RIGOUR

This Declaration acknowledges that this paper adheres to the principles for transparent reporting and scientific rigour of preclinical research as stated in the *BJP* guidelines for Design and Analysis, Immunoblotting and Immunochemistry, and Animal Experimentation, and as recommended by funding agencies, publishers and other organizations engaged with supporting research.

ORCID

Laura Moreno-Martinez https://orcid.org/0000-0002-7277-4318
Núria Gaja-Capdevila https://orcid.org/0000-0002-0028-570X
Laura Mosqueira-Martín https://orcid.org/0000-0002-5714-7682
Mireia Herrando-Grabulosa https://orcid.org/0000-0002-6685-3220
Laura Rodriguez-Gomez https://orcid.org/0000-0002-3789-3370
Ana C. Calvo https://orcid.org/0000-0001-5193-7782
Maialen Sagartzazu-Aizpurua https://orcid.org/0000-0003-3711-9884
Leticia Moreno-García https://orcid.org/0000-0003-2436-7205
Jose Manuel Fuentes https://orcid.org/0000-0001-6910-2089
Abraham Acevedo-Arozena https://orcid.org/0000-0001-6127-7116
Jesús María Aizpurua https://orcid.org/0000-0002-1053-5776
José Ignacio Miranda https://orcid.org/0000-0002-7646-6857
Ainara Vallejo-Illarramendi https://orcid.org/0000-0002-2409-8263
Xavier Navarro https://orcid.org/0000-0001-9849-902X
Rosario Osta https://orcid.org/0000-0001-5687-6704
Francisco Javier Gil-Bea https://orcid.org/0000-0003-2002-5531

REFERENCES

Aizpurua, J. M., Miranda, J. I., Irastorza, A., Torres, E., Eceiza, M., Sagartzazu-Aizpurua, M., Ferrón, P., Aldanondo, G., Lasa-Fernández, H., Marco-Moreno, P., Dadie, N., López, A., & Vallejo-Illarramendi, A. (2021). Discovery of a novel family of FKBP12 'reshapers' and their use as calcium modulators in skeletal muscle under nitro-oxidative stress. *European Journal of Medicinal Chemistry*, *213*, 113160. https://doi.org/10.1016/j.ejmech.2021.113160

Alexander, S. P. H., Fabbro, D., Kelly, E., Mathie, A. A., Peters, J. A., Veale, E. L., Armstrong, J. F., Faccenda, E., Harding, S. D., Davies, J. A., Annett, S., Boison, D., Burns, K. E., Dessauer, C., Gertsch, J., Helsby, N. A., Izzo, A. A., Ostrom, R., Papapetropoulos, A., … Wong, S. S. (2023). The concise guide to PHARMACOLOGY 2023/24: Enzymes. *British Journal of Pharmacology*, *180*(Suppl 2), S289–S373.

Alexander, S. P. H., Mathie, A. A., Peters, J. A., Veale, E. L., Striessnig, J., Kelly, E., Armstrong, J. F., Faccenda, E., Harding, S. D., Davies, J. A., Aldrich, R. W., Attali, B., Baggetta, A. M., Becirovic, E., Biel, M., Bill, R. M., Caceres, A. I., Catterall, W. A., Conner, A. C., … Zhu, M. (2023). The concise guide to PHARMACOLOGY 2023/24: Ion channels. *British Journal of Pharmacology*, *180*(Suppl 2), S145–S222. https://doi.org/10.1111/bph.16178

Alexander, S. P. H., Roberts, R. E., Broughton, B. R. S., Sobey, C. G., George, C. H., Stanford, S. C., Cirino, G., Docherty, J. R., Giembycz, M. A., Hoyer, D., Insel, P. A., Izzo, A. A., Ji, Y., MacEwan, D. J., Mangum, J., Wonnacott, S., & Ahluwalia, A. (2018). Goals and practicalities of immunoblotting and immunohistochemistry: A guide for submission to the *British Journal of Pharmacology*. *British Journal of Pharmacology*, *175*, 407–411. https://doi.org/10.1111/bph.14112

Alexianu, M. E., Ho, B. -K., Mohamed, A. H., la Bella, V., Smith, R. G., & Appel, S. H. (1994). The role of calcium-binding proteins in selective motoneuron vulnerability in amyotrophic lateral sclerosis. *Annals of Neurology*, *36*, 846–858. https://doi.org/10.1002/ana.410360608

Appel, S. H., Beers, D., Siklos, L., Engelhardt, J. I., & Mosier, D. R. (2001). Calcium: The Darth Vader of ALS. *Amyotrophic Lateral Sclerosis and Other Motor Neuron Disorders*, *2*, 47–54.

Bachmanov, A. A., Reed, D. R., Beauchamp, G. K., & Tordoff, M. G. (2002). Food intake, water intake, and drinking spout side preference of 28 mouse strains. *Behavior Genetics*, *32*, 435–443. https://doi.org/10.1023/A:1020884312053

Bergmann, F., & Keller, B. U. (2004). Impact of mitochondrial inhibition on excitability and cytosolic Ca2+ levels in brainstem motoneurones from mouse. *The Journal of Physiology*, *555*, 45–59. https://doi.org/10.1113/jphysiol.2003.053900

Bernard-Marissal, N., Médard, J.-J., Azzedine, H., & Chrast, R. (2015). Dysfunction in endoplasmic reticulum-mitochondria crosstalk underlies SIGMAR1 loss of function mediated motor neuron degeneration. *Brain*, *138*, 875–890. https://doi.org/10.1093/brain/awv008

Bursch, F., Kalmbach, N., Naujock, M., Staege, S., Eggenschwiler, R., Abo-Rady, M., Japtok, J., Guo, W., Hensel, N., Reinhardt, P., Boeckers, T. M., Cantz, T., Sterneckert, J., van den Bosch, L., Hermann, A., Petri, S., & Wegner, F. (2019). Altered calcium dynamics and glutamate receptor properties in iPSC-derived motor neurons from ALS patients with C9orf72, FUS, SOD1 or TDP43 mutations. *Human Molecular Genetics*, *28*, 2835–2850. https://doi.org/10.1093/hmg/ddz107

Dafinca, R., Barbagallo, P., Farrimond, L., Candalija, A., Scaber, J., Ababneh, N. A., Sathyaprakash, C., Vowles, J., Cowley, S., & Talbot, K. (2020). Impairment of mitochondrial calcium buffering links mutations in C9ORF72 and TARDBP in iPS-derived motor neurons from patients with ALS/FTD. *Stem Cell Reports*, *14*, 892–908. https://doi.org/10.1016/j.stemcr.2020.03.023

De Vos, K. J., Mórotz, G. M., Stoica, R., Tudor, E. L., Lau, K. F., Ackerley, S., Warley, A., Shaw, C. E., & Miller, C. C. (2012). VAPB interacts with the mitochondrial protein PTPIP51 to regulate calcium homeostasis. *Human Molecular Genetics*, *21*, 1299–1311.

Defranchi, E., Novellino, A., Whelan, M., Vogel, S., Ramirez, T., van Ravenzwaay, B., & Landsiedel, R. (2011). Feasibility assessment of micro-electrode Chip assay as a method of detecting neurotoxicity in vitro. *Frontiers in Neuroengineering*, *4*, 1–12.

Dekkers, J., Bayley, P., Dick, J. R. T., Schwaller, B., Berchtold, M. W., & Greensmith, L. (2004). Over-expression of parvalbumin in transgenic mice rescues motoneurons from injury-induced cell death. *Neuroscience*, *123*, 459–466. https://doi.org/10.1016/j.neuroscience.2003.07.013

Elliott, J. L., & Snider, W. D. (1995). Parvalbumin is a marker of ALS-resistant motor neurons. *Neuroreport*, *6*, 449–452. https://doi.org/10.1097/00001756-199502000-00011

Fabiato, A. (1983). Calcium-induced release of calcium from the cardiac sarcoplasmic reticulum. *American Journal of Physiology. Cell Physiology*, *245*, C1–C14. https://doi.org/10.1152/ajpcell.1983.245.1.C1

Fauconnier, J., Thireau, J., Reiken, S., Cassan, C., Richard, S., Matecki, S., Marks, A. R., & Lacampagne, A. (2010). Leaky RyR2 trigger ventricular arrhythmias in Duchenne muscular dystrophy. *Proceedings of the National Academy of Sciences of the United States of America*, *107*, 1559–1564. https://doi.org/10.1073/pnas.0908540107

Gaja-Capdevila, N., Hernández, N., Navarro, X., & Herrando-Grabulosa, M. (2021). Sigma-1 receptor is a pharmacological target to promote neuroprotection in the SOD1G93A ALS mice. *Frontiers in Pharmacology*, *12*, 780588. https://doi.org/10.3389/fphar.2021.780588

Gan, S., Yin, J., Yao, Y., Liu, Y., Chang, D., Zhu, D., & Shi, L. (2017). Metal- and additive-free oxygen-atom transfer reaction: An efficient and chemoselective oxidation of sulfides to sulfoxides with cyclic diacyl peroxides. *Organic & Biomolecular Chemistry*, *15*, 2647–2654. https://doi.org/10.1039/C7OB00021A

Guatteo, E., Carunchio, I., Pieri, M., Albo, F., Canu, N., Mercuri, N. B., & Zona, C. (2007). Altered calcium homeostasis in motor neurons following AMPA receptor but not voltage-dependent calcium channels' activation in a genetic model of amyotrophic lateral sclerosis. *Neurobiology of Disease*, *28*, 90–100. https://doi.org/10.1016/j.nbd.2007.07.002

Heiman-Patterson, T. D., Deitch, J. S., Blankenhorn, E. P., Erwin, K. L., Perreault, M. J., Alexander, B. K., Byers, N., Toman, I., & Alexander, G. M. (2005). Background and gender effects on survival in the TgN (SOD1-G93A)1Gur mouse model of ALS. *Journal of the Neurological Sciences*, *236*, 1–7. https://doi.org/10.1016/j.jns.2005.02.006

Ho, B. K., Alexianu, M. E., Colom, L. V., Mohamed, A. H., Serrano, F., & Appel, S. H. (1996). Expression of calbindin-D28K in motoneuron hybrid cells after retroviral infection with calbindin-D28K cDNA prevents amyotrophic lateral sclerosis IgG-mediated cytotoxicity. *Proceedings of the National Academy of Sciences of the United States of America*, *93*, 6796–6801. https://doi.org/10.1073/pnas.93.13.6796

Ince, P., Stout, N., Shaw, P., Slade, J., Hunziker, W., Heizmann, C. W., & Baimbridge, K. G. (1993). Parvalbumin and calbindin D-28k in the human motor system and in motor neuron disease. *Neuropathology and Applied Neurobiology*, *19*, 291–299. https://doi.org/10.1111/j.1365-2990.1993.tb00443.x

Jaiswal, M. K. (2013). Calcium, mitochondria, and the pathogenesis of ALS: The good, the bad, and the ugly. *Frontiers in Cellular Neuroscience*, *7*, 199. https://doi.org/10.3389/fncel.2013.00199

Kihira, T., Utunomiya, H., & Kondo, T. (2005). Expression of FKBP12 and ryanodine receptors (RyRs) in the spinal cord of MND patients. *Amyotrophic Lateral Sclerosis and Other Motor Neuron Disorders*, *6*, 94–99. https://doi.org/10.1080/14660820510034442

Komine, O., Yamashita, H., Fujimori-Tonou, N., Koike, M., Jin, S., Moriwaki, Y., Endo, F., Watanabe, S., Uematsu, S., Akira, S., Uchiyama, Y., Takahashi, R., Misawa, H., & Yamanaka, K. (2018). Innate immune adaptor TRIF deficiency accelerates disease progression of ALS mice with accumulation of aberrantly activated astrocytes. *Cell*

Death and Differentiation, *25*, 2130–2146. https://doi.org/10.1038/s41418-018-0098-3

Lacampagne, A., Liu, X., Reiken, S., Bussiere, R., Meli, A. C., Lauritzen, I., Teich, A. F., Zalk, R., Saint, N., Arancio, O., Bauer, C., Duprat, F., Briggs, C. A., Chakroborty, S., Stutzmann, G. E., Shelanski, M. L., Checler, F., Chami, M., & Marks, A. R. (2017). Post-translational remodeling of ryanodine receptor induces calcium leak leading to Alzheimer's disease-like pathologies and cognitive deficits. *Acta Neuropathologica*, *134*, 749–767. https://doi.org/10.1007/s00401-017-1733-7

Leal, S. S., & Gomes, C. M. (2015). Calcium dysregulation links ALS defective proteins and motor neuron selective vulnerability. *Frontiers in Cellular Neuroscience*, *9*, 225.

Lehnart, S. E., Mongillo, M., Bellinger, A., Lindegger, N., Chen, B. X., Hsueh, W., Reiken, S., Wronska, A., Drew, L. J., Ward, C. W., Lederer, W. J., Kass, R. S., Morley, G., & Marks, A. R. (2008). Leaky Ca2+ release channel/ryanodine receptor 2 causes seizures and sudden cardiac death in mice. *The Journal of Clinical Investigation*, *118*, 2230–2245. https://doi.org/10.1172/JCI35346

LeMasson, G., Przedborski, S., & Abbott, L. F. (2014). A computational model of motor neuron degeneration. *Neuron*, *83*, 975–988. https://doi.org/10.1016/j.neuron.2014.07.001

Lilley, E., Stanford, S. C., Kendall, D. E., Alexander, S. P. H., Cirino, G., Docherty, J. R., George, C. H., Insel, P. A., Izzo, A. A., Ji, Y., Panettieri, R. A., Sobey, C. G., Stefanska, B., Stephens, G., Teixeira, M., & Ahluwalia, A. (2020). ARRIVE 2.0 and the British Journal of Pharmacology: Updated guidance for 2020. *British Journal of Pharmacology*, *177*(16), 3611–3616. Portico. https://doi.org/10.1111/bph.15178

Liu, X., Betzenhauser, M. J., Reiken, S., Meli, A. C., Xie, W., Chen, B. X., Arancio, O., & Marks, A. R. (2012). Role of leaky neuronal ryanodine receptors in stress- induced cognitive dysfunction. *Cell*, *150*, 1055–1067. https://doi.org/10.1016/j.cell.2012.06.052

Mancuso, R., Oliván, S., Mancera, P., Pastén-Zamorano, A., Manzano, R., Casas, C., Osta, R., & Navarro, X. (2012). Effect of genetic background on onset and disease progression in the SOD1-G93A model of amyotrophic lateral sclerosis. *Amyotrophic Lateral Sclerosis*, *13*, 302–310. https://doi.org/10.3109/17482968.2012.662688

Mancuso, R., Santos-Nogueira, E., Osta, R., & Navarro, X. (2011). Electrophysiological analysis of a murine model of motoneuron disease. *Clinical Neurophysiology*, *122*, 1660–1670. https://doi.org/10.1016/j.clinph.2011.01.045

McPhersonx, P. S., Kim, Y. K., Valdivia, H., Knudson, C. M., Takekura, H., Franzini-Armstrong, C., Coronadot, R., & Campbell, K. P. (1991). The brain ryanodine receptor: A caffeine-sensitive calcium release channel. *Neuron*, *7*, 17–25. https://doi.org/10.1016/0896-6273(91)90070-G

Mead, R. J., Shan, N., Reiser, H. J., Marshall, F., & Shaw, P. J. (2023). Amyotrophic lateral sclerosis: A neurodegenerative disorder poised for successful therapeutic translation. *Nature Reviews. Drug Discovery*, *22*, 185–212. https://doi.org/10.1038/s41573-022-00612-2

Murayama, T., Kurebayashi, N., Yamazawa, T., Oyamada, H., Suzuki, J., Kanemaru, K., Oguchi, K., Iino, M., & Sakurai, T. (2015). Divergent activity profiles of type 1 ryanodine receptor channels carrying malignant hyperthermia and central Core disease mutations in the amino-terminal region. *PLoS ONE*, *10*, e0130606. https://doi.org/10.1371/journal.pone.0130606

Nguyen, M. D., D'Aigle, T., Gowing, G., Julien, J. P., & Rivest, S. (2004). Exacerbation of motor neuron disease by chronic stimulation of innate immunity in a mouse model of amyotrophic lateral sclerosis. *Journal of Neuroscience*, *24*, 1340–1349. https://doi.org/10.1523/JNEUROSCI.4786-03.2004

Paizs, M., Tortarolo, M., Bendotti, C., Engelhardt, J. I., & Siklós, L. (2011). Talampanel reduces the level of motoneuronal calcium in transgenic mutant SOD1 mice only if applied presymptomatically. *Amyotrophic Lateral Sclerosis*, *12*, 340–344. https://doi.org/10.3109/17482968.2011.584627

Passannante, R., Gómez-Vallejo, V., Sagartzazu-Aizpurua, M., Vignau Arsuaga, L., Marco-Moreno, P., Aldanondo, G., Vallejo-Illarramendi, A., Aguiar, P., Cossío, U., Martín, A., Bergare, J., Kingston, L., Elmore, C. S., Morcillo, M. A., Ferrón, P., Aizpurua, J. M., & Llop, J. (2023). Pharmacokinetic evaluation of new drugs using a multi-labelling approach and PET imaging: Application to a drug candidate with potential application in neuromuscular disorders. *Biomedicine*, *11*, 253. https://doi.org/10.3390/biomedicines11020253

Percie du Sert, N., Hurst, V., Ahluwalia, A., Alam, S., Avey, M. T., Baker, M., Browne, W. J., Clark, A., Cuthill, I. C., Dirnagl, U., Emerson, M., Garner, P., Holgate, S. T., Howells, D. W., Karp, N. A., Lazic, S. E., Lidster, K., MacCallum, C. J., Macleod, M., … Würbel, H. (2020). The ARRIVE guidelines 2.0: Updated guidelines for reporting animal research. *PLOS Biology*, *18*(7), e3000410. https://doi.org/10.1371/journal.pbio.3000410

Peters, L. R., & Raghavan, M. (2011). Endoplasmic reticulum calcium depletion impacts chaperone secretion, innate immunity, and phagocytic uptake of cells. *Journal of Immunology*, *187*, 919–931. https://doi.org/10.4049/jimmunol.1100690

Petrozziello, T., Boscia, F., Tedeschi, V., Pannaccione, A., de Rosa, V., Corvino, A., Severino, B., Annunziato, L., & Secondo, A. (2022). Na+/Ca2+ exchanger isoform 1 takes part to the Ca2+−related prosurvival pathway of SOD1 in primary motor neurons exposed to beta-methylamino-L-alanine. *Cell Communication and Signaling: CCS*, *20*, 8. https://doi.org/10.1186/s12964-021-00813-z

Shaffer, C. L. (2010). Defining Neuropharmacokinetic parameters in CNS drug discovery to determine cross-species pharmacologic exposure–response relationships. *Annual Reports in Medicinal Chemistry*, *45*, 55–70. https://doi.org/10.1016/S0065-7743(10)45004-6

Staats, K. A., Van Rillaer, M., Scheveneels, W., Verbesselt, R., Van Damme, P., Robberecht, W., & Van Den Bosch, L. (2012). Dantrolene is neuroprotective in vitro, but does not affect survival in SOD1G93A mice. *Neuroscience*, *220*, 26–31. https://doi.org/10.1016/j.neuroscience.2012.06.050

Tadic, V., Prell, T., Lautenschlaeger, J., & Grosskreutz, J. (2014). The ER mitochondria calcium cycle and ER stress response as therapeutic targets in amyotrophic lateral sclerosis. *Frontiers in Cellular Neuroscience*, *8*, 147.

Turner, B. J., & Talbot, K. (2008). Transgenics, toxicity and therapeutics in rodent models of mutant SOD1-mediated familial ALS. *Progress in Neurobiology*, *85*, 94–134. https://doi.org/10.1016/j.pneurobio.2008.01.001

Vanselow, B. K., & Keller, B. U. (2000). Calcium dynamics and buffering in oculomotor neurones from mouse that are particularly resistant during amyotrophic lateral sclerosis (ALS)-related motoneurone disease. *The Journal of Physiology*, *525*(2), 433–445. https://doi.org/10.1111/j.1469-7793.2000.t01-1-00433.x

Yao, J., Liu, Y., Sun, B., Zhan, X., Estillore, J. P., Turner, R. W., & Chen, S. R. W. (2022). Increased RyR2 open probability induces neuronal hyperactivity and memory loss with or without Alzheimer's disease–causing gene mutations. *Alzheimer's & Dementia*, *18*, 2088–2098. https://doi.org/10.1002/alz.12543

Yao, J., Sun, B., Institoris, A., Zhan, X., Guo, W., Song, Z., Liu, Y., Hiess, F., Boyce, A. K. J., Ni, M., Wang, R., ter Keurs, H., Back, T. G., Fill, M., Thompson, R. J., Turner, R. W., Gordon, G. R., & Chen, S. R. W. (2020). Limiting RyR2 open time prevents Alzheimer's disease-related neuronal hyperactivity and memory loss but not β-amyloid accumulation. *Cell Reports*, *32*, 108169. https://doi.org/10.1016/j.celrep.2020.108169

Zhang, Y., Huo, M., Zhou, J., & Xie, S. (2010). PKSolver: An add-in program for pharmacokinetic and pharmacodynamic data analysis in Microsoft excel. *Computer Methods and Programs in Biomedicine*, *99*, 306–314. https://doi.org/10.1016/j.cmpb.2010.01.007

Zhou, W., & Xu, R. (2023). Current insights in the molecular genetic pathogenesis of amyotrophic lateral sclerosis. *Frontiers in Neuroscience*, *17*, 1189470. https://doi.org/10.3389/fnins.2023.1189470

Zima, A. V., & Mazurek, S. R. (2016). Functional impact of ryanodine receptor oxidation on intracellular calcium regulation in the heart. *Reviews of Physiology, Biochemistry and Pharmacology*, *171*, 39–62. https://doi.org/10.1007/112_2016_2

SUPPORTING INFORMATION

Additional supporting information can be found online in the Supporting Information section at the end of this article.

How to cite this article: Moreno-Martinez, L., Gaja-Capdevila, N., Mosqueira-Martín, L., Herrando-Grabulosa, M., Rodriguez-Gomez, L., Gonzalez-Imaz, K., Calvo, A. C., Sagartzazu-Aizpurua, M., Moreno-García, L., Fuentes, J. M., Acevedo-Arozena, A., Aizpurua, J. M., Miranda, J. I., López de Munain, A., Vallejo-Illarramendi, A., Navarro, X., Osta, R., & Gil-Bea, F. J. (2025). Novel FKBP prolyl isomerase 1A (FKBP12) ligand promotes functional improvement in SOD1^{G93A} amyotrophic lateral sclerosis (ALS) mice. *British Journal of Pharmacology*, 1–21. https://doi.org/10.1111/bph.17448